Pharmacological Research 183 (2022) 106375

Contents lists available at ScienceDirect

Pharmacological Research

journal homepage: www.elsevier.com/locate/yphrs

Rabphilin-3A as a novel target to reverse α-synuclein-induced synaptic loss in Parkinson's disease

Elena Ferrari [a], Diego Scheggia [a], Elisa Zianni [a], Maria Italia [a], Marta Brumana [a], Luca Palazzolo [a], Chiara Parravicini [a], Andrea Pilotto [b], Alessandro Padovani [b], Elena Marcello [a], Ivano Eberini [a], Paolo Calabresi [c,d], Monica Diluca [a], Fabrizio Gardoni [a,*]

[a] Department of Pharmacological and Biomolecular Sciences (DiSFeB), University of Milan, 20133 Milan, Italy
[b] Neurology Unit, Department of Clinical and Experimental Sciences, University of Brescia, 25123 Brescia, Italy
[c] Sezione di Neurologia, Dipartimento di Neuroscienze, Facoltà di Medicina e Chirurgia, Università Cattolica del Sacro Cuore, Rome, Italy
[d] Sezione di Neurologia, Dipartimento di Neuroscienze, Facoltà di Medicina e Chirurgia, Università Cattolica del Sacro Cuore, Rome, Italy

ARTICLE INFO

Keywords:
α-synuclein
Dendritic spines
Parkinson's disease
Protein-protein interactions
Rabphilin-3A
Mice

ABSTRACT

Toxic aggregates of α-synuclein (αsyn) are considered key drivers of Parkinson's disease (PD) pathology. In early PD, αsyn induces synaptic dysfunction also modulating the glutamatergic neurotransmission. However, a more detailed understanding of the molecular mechanisms underlying αsyn-triggered synaptic failure is required to design novel therapeutic interventions. Here, we described the role of Rabphilin-3A (Rph3A) as novel target to counteract αsyn-induced synaptic loss in PD. Rph3A is a synaptic protein interacting with αsyn and involved in stabilizing dendritic spines and in promoting the synaptic retention of NMDA-type glutamate receptors. We found that *in vivo* intrastriatal injection of αsyn-preformed fibrils in mice induces the early loss of striatal synapses associated with decreased synaptic levels of Rph3A and impaired Rph3A/NMDA receptors interaction. Modulating Rph3A striatal expression or interfering with the Rph3A/αsyn complex with a small molecule prevented dendritic spine loss and rescued associated early motor defects in αsyn-injected mice. Notably, the same experimental approaches prevented αsyn-induced synaptic loss *in vitro* in primary hippocampal neurons. Overall, these findings indicate that approaches aimed at restoring Rph3A synaptic functions can slow down the early synaptic detrimental effects of αsyn aggregates in PD.

1. Introduction

Parkinson's disease (PD) is the second most common neurodegenerative disorder [1]. The disease is mainly characterized by the progressive loss of dopaminergic neurons in the *substantia nigra pars compacta* (SNpc) and the abnormal accumulation and aggregation of α-synuclein (αsyn) in the form of Lewy bodies and Lewy neurites [2–4]. Additional mechanisms, including inflammatory events, oxidative stress, and mitochondrial dysfunction also contribute to disease progression.

Aberrant levels and forms of αsyn can trigger neurotoxic events through multiple mechanisms affecting homeostatic cell pathways and synaptic functions. In particular, recent experimental evidence obtained in both *in vivo* and *in vitro* models demonstrates the impact of αsyn oligomers and αsyn-preformed fibrils (αsyn-PFF) on glutamatergic synaptic transmission in early stages of disease progression before a full blown neurodegeneration occurred [5,6]. Asyn oligomers were shown to block the induction of long-term potentiation (LTP) in hippocampal [7] and corticostriatal slices [6]. Similarly, *in vivo* injection of αsyn-PFF in rodents induced the loss of LTP and long-term depression (LTD) at corticostriatal synapses 12 weeks after injection [5]. Along with the well-known role of NMDA receptor (NMDAR) function in the induction

Abbreviations: AMPAR, alpha-amino-3-hydroxy-5-methyl-4-isoxazolepropionate receptor; αsyn, α-synuclein; BSA, Bovine serum albumin; DAPI, 4′,6-diamidino-2-phenylindole; DAT, dopamine transporter; DIV, day *in vitro*; dpi, days post injection; GFP, green fluorescent protein; LTD, long-term depression; LTP, long-term potentiation; NMDAR, N-methyl-D-aspartate receptor; OD, optical density; PLA, proximity ligation assay; Rph3A, Rabphilin-3A; SIM, structured illumination microscopy; SNpc, substantia nigra pars compacta; SPN, striatal projection neuron; TH, tyrosine hydroxylase; TIF, triton-insoluble postsynaptic fraction; αsyn-PFF, αsyn-preformed fibrils.

* Correspondence to: Department of Pharmacological and Biomolecular Sciences, University of Milan, Via Balzaretti 9, 20133 Milan, Italy.
E-mail address: fabrizio.gardoni@unimi.it (F. Gardoni).

https://doi.org/10.1016/j.phrs.2022.106375
Received 4 July 2022; Received in revised form 24 July 2022; Accepted 27 July 2022
Available online 30 July 2022

of synaptic plasticity at glutamatergic synapses, several reports in the last decade have demonstrated a direct effect of αsyn on synaptic NMDAR. Increased levels of cellular αsyn caused NMDAR internalization [7,8], which was increased by αsyn oligomerization [9]. Similar studies confirmed that αsyn activity promoted endocytosis of NMDARs [10,11]. In particular, reduced NMDAR currents in striatal projection neurons (SPNs) are mainly associated with a reduced postsynaptic localization of the GluN2A subunit [6]. Finally, Tozzi and coworkers identified a specific pathogenic mechanism induced by αsyn oligomers on GluN2D-containing NMDARs in striatal cholinergic interneurons [12]. Despite these studies agree to point at postsynaptic NMDARs as targets for early αsyn-mediated synaptic toxicity, the molecular mechanisms involved in these processes remain unknown, and potential treatment strategies are lacking.

Rabphilin-3A (Rph3A) is a synaptic protein initially known as a synaptic vesicle-associated protein involved in the regulation of exo- and endocytosis processes at presynaptic sites [13,14]. At excitatory dendritic spines, Rph3A is required for the synaptic retention of NMDARs through direct interaction with the GluN2A regulatory subunit [15–17]. Formation of the Rph3A complex with NMDAR is also needed for the molecular and structural modification of dendritic spines induced by LTP, and accumulation of Rph3A in potentiated spines has been observed [15]. Conversely, Rph3A silencing induces spine loss and prevents the activity-dependent formation of new spines [15]. Notably, Rph3A has been involved in the pathogenesis of different neurodegenerative disorders. Several reports using various *in vitro* and *in vivo* models converge in indicating the downregulation of Rph3A expression as a culprit of synaptic dysfunction and early neurodegeneration [18–21]. Imaging studies showed Rph3A enrichment at the dendritic spines of SPNs [22]. MPTP-treated monkeys exhibited significantly decreased Rph3A mRNA levels in the caudate, putamen, and medial and superior frontal gyrus and reduced Rph3A mRNA was also found in the superior frontal gyrus of post-mortem brain samples from PD patients [22]. Interestingly, aberrant Rph3A synaptic localization plays a key role in L-DOPA-induced dyskinesias associated with increased NMDAR activity [22]. However, very few data are available on a possible involvement of Rph3A in αsyn-mediated pathology in early stages of PD. The formation of αsyn/Rph3A protein complex has been proposed [23] and injection of AAV-αsyn-A53T induced modifications of striatal Rph3A levels [24].

In this study, we used the αsyn-PFF mouse model [25] to (i) evaluate the role of Rph3A and its interaction with αsyn in the onset of early detrimental effects induced by αsyn aggregates at striatal synapses and (ii) evaluate Rph3A modulation as novel therapeutic strategy to counteract αsyn-mediated early glutamatergic dysfunctions.

Our results show that both Rph3A overexpression and the use of a small molecule able to interfere with the Rph3A/αsyn complex fully prevented SPN dendritic spine loss and its associated early motor defects in αsyn-PFF mice. Importantly, *in vivo* results were replicated *in vitro* in primary hippocampal neurons, affirming Rph3A's role in mediating αsyn synaptic toxicity in different brain areas.

2. Methods

2.1. Molecular modeling

Compounds to evaluate for their ability to bind the target Rph3A region and, consequently, to interfere with the Rph3A/αsyn complex were chosen from 1. the *Asinex BioDesign* library of molecules with key structural features of known pharmacologically relevant natural products on feasible medicinal chemistry scaffolds and 2. the *Asinex Gold & Platinum* library, in which most compounds are highly similar to drugs (http://www.asinex.com).

The charge-related molecular descriptors "F_charge" (the total charge of the molecule less the sum of formal charges) and "a_acid" (the number of acidic atoms) used to build the starting library of 1545 acidic compounds were calculated with molecular operating environment (MOE) software using the QuaSAR-Descriptor tool.

The molecular docking of all the investigated compounds was conducted on a homology model of human Rph3A that included two calcium ions and an IP_3 molecule, built from 2CM5, 5LOB, 5LOW, and 5LO8 rat crystallographic structures (obtained from RCSB PDB) using the Amber12:EHT force field (see Fig. S1). In particular, using MOE software, PDB structures corresponding to rat Rph3A 2CM5, 5LOB, 5LOW and 5LO8 were aligned and the best structure in terms of sequence coverage and co-crystalized ligands was kept (*i.e.*, 5LO8. B). Ca^{2+} ions, included in 2CM5 structure, and PIP2, co-crystalized in PDB 5LO8, were both added to the model. The protein was prepared in the Automated Structure Preparation program [https://www.chemcomp.com/Products.htm] of the MOE, to check and correct structures for subsequent computational analysis. The database of compounds to be investigated was processed with the Energy Minimize program using the default parameters of the MOE Compute module to produce a single low-energy conformation for each putative ligand.

The *in-silico* screening was conducted in the MOE Dock program contained in the Compute module, following Eberini and coworkers workflow [26]. The full Rph3A model structure was set as receptor and the binding site was defined from Ser618 to Lys663.

Conformations for each ligand were generated by sampling their rotatable bonds. Triangle Matcher was the placement methodology selected. The generated poses were scored according to the London dG, an empirical scoring function that estimates the approximate binding free energy of ligand from a given pose. The 30 top-scoring poses continued to a refinement step based on molecular mechanics and were rescored according to the GBVI/WSA dG, a force-field-based empirical scoring function that estimates the approximate binding free energy of ligand from a given pose.

Docking simulations were also performed *via* Schrödinger Glide both in its standard (SP) and extra precision (XP) modes [27]. As a constraint (ligand–receptor interaction requirement), a grid of the receptor containing the bottom α-helical region of Rph3A was generated. Before the docking procedures, the Rph3A model was prepared and energy-minimized with the Protein Preparation Wizard, using the OPLS3e force field [28] of the Biologics Drug Discovery suite [https://www.schrodinger.com/platform/biologics-drug-discovery]. The same force field was applied in all the molecular docking procedures. The binding free energy of the complexes produced by the molecular docking pipeline was evaluated *via* the Glide XP Score, which was empirically generated to approximate the ligand binding free energy, to separate putative ligands from non-ligands.

The pharmacokinetic properties of the final library of molecules were predicted with the ACD/Percepta ADME Suite (ACD/Labs, Toronto, Canada) through a combination of quantitative structure–activity relationship (QSAR) models.

2.2. Preparation of αsyn-PFF

αsyn-PFF were generated *in vitro* from recombinant αsyn monomeric protein (Proteos, MI, USA) using a validated protocol, with some modifications [5,29]. Monomeric protein solution (10 mg/ml) was thawed on ice and then centrifuged at 13,000xg for 10 min at 4 °C and any pelleted protein was discarded. The supernatant was retained, and its protein concentration was measured with a Bradford assay. The solution was then diluted in phosphate-buffered saline (PBS) to a concentration of 5 mg/ml and incubated in benchtop tubes for 7 days at 37 °C with constant shaking (1000 rpm) using an Eppendorf Thermomixer. After this period, fibril (αsyn-PFF) formation was checked with transmission electron microscopy (TEM) using a Talos L120C (Thermo Fischer, USA) at 120 kV. Digital images were acquired with a CETA-MTM 4k x 4k camera (Thermo Fischer, USA). TEM analyses were performed at the Unitech NOLIMITS imaging facility of the University of Milan. The αsyn-PFF were then diluted to a final concentration of 2 mg/ml, aliquoted, and stored at − 80 °C. Immediately before experimental use,

αsyn-PFF aliquots were thawed at room temperature (RT) and sonicated for 60 pulses (2 s on/1 s off) in an ultrasonic bath sonicator (Bransonic M2800H-E). An aliquot of sonicated αsyn-PFF was examined again by the negative staining protocol with TEM [5].

2.3. Animals

All procedures involving animals were approved by the local Animal Use Committee and the Italian Ministry of Health (permits 1200/2020-PR, 330/2018-PR and 5247B.N.YCK2018) and were conducted following the National Institutes of Health *Guide for the Care and Use of Laboratory Animals* and the European Community Council Directives 2010/63/EU.

Two to four 2-month-old C57BL/6J male mice were housed in cages in a climate-controlled facility (22 ± 2 °C), with *ad libitum* access to food and water throughout and a 12 h light–dark cycle (19:00–07:00 schedule). Experiments were run during the light phase (between 10:00 and 17:00). All mice were handled on alternate days during the week preceding the first behavioral testing. Distinct cohorts of mice were used for each experimental approach (behavioral tasks, spine morphology, and biochemistry).

2.4. Surgical procedures

C57BL/6 J male mice were anesthetized with a mix of isoflurane (2 %) and oxygen (1.5 %) by inhalation and mounted in a stereotaxic frame (Kopf Instruments) linked to a digital micromanipulator. A small incision was made to expose the skull and bilateral holes were made with a drill above the targeted injection sites. The brain coordinates, taken relative to the bregma, of bilateral injection into the dorsal striatum were chosen as previously described [25]: anterior–posterior (AP), + 0.2 mm; medial–lateral (ml): ± 2 mm; and dorsal–ventral (DV): − 2.6 mm. Mice were injected with 2.5 μl of αsyn-PFF (5 μg) or PBS, infused through a 10 μl Hamilton syringe using a microinjection pump at a flow rate of 0.25 μl/min; at the end of the injection, the needle was left in place for 4 min to allow the solution to flow out entirely.

To achieve Rph3A overexpression, 35 days post-injection (dpi) of αsyn-PFF, a group of mice was injected with adeno-associated virus serotype 9 (AAV9) carrying the plasmid construct hSyn-GFP-Rph3A-WPRE (1,1 × 10^14 vg/ml) or the control hSyn-GFP-WPRE (1,4 × 10^14 vg/ml). Recombinant AAV-vectors were produced and purchased from ICGEB (Trieste, Italy). 2 μl of virus solution was infused bilaterally (flow rate of 0.2 μl/min) at the same brain coordinates for the dorsal striatum described above. After recovering from the surgical procedures, mice received carprofen (5 mg/kg) in their drinking water for 3 consecutive days.

At dpi65 of αsyn-PFF or PBS, a guide cannula was implanted in the lateral cerebral ventricle through stereotaxic surgery. After the incision, skin was removed, and a small unilateral craniotomy was performed to allow the placement of the guide cannula. The brain coordinates for the cerebral lateral ventricle were chosen according to the mouse brain atlas: + 0.2 mm; medial–lateral (ml): ± 1 mm; and dorsal–ventral (DV): − 1.5 mm (to allow the final DV injection coordinate to be −2.5 mm). Contralateral to the cannula insertion, a small screw was placed to ensure the implant grip. Once the skull was completely dry, liquid dental cement (zinc phosphate cement powder, Dentsply) was applied around the screw and the cannula to secure them in place. The cement was allowed to completely harden and the stereotaxic arm removed, leaving the guide cannula in place. A dummy cannula was then placed on top of the internal cannula to avoid any entry of external material.

From dpi70, mice received intracerebroventricular administrations of 3 μl of Compound B (1 mM) dissolved in 5% DMSO/95% saline every 3 days. This molarity allowed an estimated concentration of about 85 μM in the cerebrospinal fluid (CSF) to be attained, considering a total CSF volume of ~35 μl in the mice [30]. An injector connected to a microinjection pump was used to infuse the solution at a constant rate of 2 μl/min. Control animals received injections of the vehicle solution only. All animals were then sacrificed 48 h after the last administration.

2.5. Open field test

To assess general locomotor activity and anxiety-like behaviors, mice were tested on the open field task for 10 min. Mice were individually placed in the center of the arena (44 × 44 cm) and video-tracking software (ANY-maze, Ugo Basile, Italy) was used to record and analyze their movements. The distance traveled and time spent at the center and corners of the arena were automatically calculated by the ANY-maze software.

2.6. Rotarod test

To assess motor learning, coordination and balance, mice were tested on a rotarod apparatus (Ugo Basile) using an already described protocols with some modifications [25,31]. To familiarize them with the instrument, each mouse was given training sessions (three trials/day for a maximum of 300 s/trial) for 3 days before the testing days. Each test session was composed of three consecutive trials of the duration of maximum 300 s with 2 min as inter-trial interval; the trial was stopped as the mouse fell off the rod. For the accelerating rotarod test, each mouse was placed on the rotarod with the speed increasing from 20 rpm to 40 rpm. For the constant speed test the rotarod was set at 30 rpm. The latency to fall off the rod was recorded for each mouse in each test and the mean of the duration of three consecutive trials was used in the analysis.

2.7. Grip strength test

Forelimb muscle strength was tested with a grip strength test using a grip strength meter (Ugo Basile). Mice were held by the tails, brought close to the bar longitudinally, and allowed to grasp it. Mice were gently pulled away from the bar while the peak force (*g*) they applied was recorded. Each mouse was tested in five consecutive trials. After each trial, the animal was allowed to rest for 1 min

2.8. Spine morphology

For *ex-vivo* confocal imaging of dendritic spines, neurons were labeled with DiI dye (Invitrogen), a fluorescent lipophilic carbocyanine dye that diffuses along the neuronal membrane, labeling fine dendritic arborization and spine structures in brain slices pre-fixed with 1.5 % PFA. The DiI labeling procedure was performed as previously described [16]. DiI solid crystals were applied with a thin needle by lightly touching the region of interest on both sides of 3-mm brain pieces comprising the striatum prepared after cardiac perfusion with 1.5 % PFA in PB 0.1 M. The DiI dye was left to diffuse for 1 day in the dark at RT, and then slices were post-fixed with 4 % PFA in PB 0.1 M for 45 min at 4 ºC. The first slice containing the DiI crystals was discarded and 100 μm striatal slices were then obtained with a vibratome and collected in PBS. Slices were mounted on Superfrost glass slides (Thermo Fisher) with Fluoroshield (Sigma) for confocal imaging. Fluorescence images were acquired with the Zeiss Confocal LSM900 system using a sequential acquisition setting at 1024 × 1,024-pixel resolution at 555 nm. For each image, between 20 and 60 sections were acquired and an appropriate z-projection was obtained. Analyses of spine morphology were performed using ImageJ software.

2.9. Primary hippocampal neuronal cultures

Primary hippocampal neuronal cultures were prepared from embryonic day-18 (E18) Sprague-Dawley rat hippocampi (Charles River, Milan, Italy) as previously described [32]. Neurons were transfected with an EGFP plasmid on the seventh *day in vitro* (*DIV7*) with the

calcium-phosphate coprecipitation method.

2.10. αsyn-PFF treatment

Before they were administered to cells, αsyn-PFF aliquots were thawed at RT, diluted in PBS to the final concentration of 0.1 μg/μl, and sonicated for 60 pulses (2 s on/1 s off) in an ultrasonic bath sonicator (Bransonic M2800H-E). At *DIV9*, αsyn-PFF were added in a single dose to the neuronal culture medium at a concentration of 1 or 2 μg/ml and left for 7 days. Control neurons were treated with the vehicle solution alone.

2.11. Compound B treatment

Compound B was added directly to the culture medium at *DIV12*. The molecule was suspended in DMSO at a concentration of 10 mM and added to the neurons in a single dose to reach the final concentration of 10 μM. The treated cultures were then left for 4 days.

2.12. Treatment of acute cortico-striatal slices with Asinex compounds

To obtain acute corticostriatal slices, adult Sprague-Dawley rats were anesthetized with a mix of isoflurane (2 %) and oxygen (1.5 %) and decapitated. The brain was rapidly removed from the skull and immersed in cold Kreb's solution containing 126 mM NaCl, 2.5 mM KCl, 1.2 mM $MgCl_2$, 2.4 mM $CaCl_2$, 1.2 mM NaH_2PO_4, 24 mM $NaHCO_3$, and 10 mM glucose, saturated with 95 % O_2/5 % CO_2 (pH 7.4). Coronal slices containing striatum and cortex were cut at 250 μm thick with a vibratome (Vibratome 1000 Plus, IMEB). Slices were maintained in Kreb's solution at RT for 30 min before treatment was administered. Then, the resting Kreb's solution was replaced with one containing 10 μM of each compound or the vehicle (DMSO) for control samples. At the end of the treatment, free-floating slices were washed with fresh Kreb's solution and the striata were quickly isolated and stored at − 80 °C for molecular assays.

2.13. Immunocytochemistry (ICC)

For colocalization and morphological studies, hippocampal neurons were fixed at *DIV16* for 15 min at RT in 4 % PFA with 4 % sucrose in Dulbecco's PBS (Sigma-Aldrich). Coverslips were then washed with PBS, permeabilized with 0.1 % Triton X-100 in PBS for 15 min at RT and blocked for 30 min at RT with 5 % bovine serum albumin (BSA) in PBS. Cells were then incubated with primary antibodies in 3 % BSA–PBS overnight at 4 ºC in a humid chamber. After washing with PBS, the cells were incubated with the fluorophore-conjugated secondary antibodies in 3 % BSA–PBS for 1 h at RT in a humid chamber in the dark. The incubation was followed by PBS washes and mounting on glass slides with Fluoroshield mounting medium (Sigma-Aldrich). For spine density, GluN2A/Rph3A Images were acquired using an inverted LSM900 confocal microscope (Zeiss) with a 63X objective and were analyzed using ImageJ software. Neurons were chosen randomly for quantification from different coverslips from independent experiments and images were acquired using the same settings/laser power.

2.14. Proximity ligation assay (PLA)

Primary hippocampal neurons were fixed at *DIV16* with 4 % PFA and 4 % sucrose for 15 min at RT in PBS. Coverslips were then washed three times with PBS and permeabilized with 0.1 % Triton-X-100 in PBS for 15 min and later blocked with 5 % BSA in PBS for 30 min at RT. Coverslips were then incubated in a dark humid chamber overnight at 4 °C with primary antibodies in 5 % BSA in PBS, washed three times with PBS, and then incubated with secondary antibodies conjugated with oligonucleotides (PLA probe MINUS and PLA probe PLUS) for 1 h at 37 °C in a dark humid chamber. Coverslips were then washed three times with PBS and incubated with the ligation solution (Olink Bioscience) supplemented with ligase (25 mU/μl) for 30 min at 37 ºC in a dark humid chamber and washed with Wash Buffer A (0.15 M NaCl, 0.01 M Tris, and 0.05 % tween 20; pH 7.4; Olink Bioscience). The amplification solution (containing nucleotides and fluorescently labeled oligonucleotides; Olink Bioscience) supplemented with polymerase (0.125 U/μl) was added to each sample and incubated for 100 min at 37 ºC in a humid dark chamber. Coverslips were then washed three times with decreasing concentrations of Wash Buffer B (0.1 M NaCl and 0.2 M Tris; pH 7.5; Olink Bioscience). Images were acquired using an inverted LSM900 confocal microscope (Zeiss) with a 63X objective and were analyzed using ImageJ software. Neurons were chosen randomly for quantification from different coverslips from independent experiments and images were acquired using the same settings/laser power.

2.15. Free-floating immunohistochemistry (IHC)

Mice were perfused with 4 % PFA in PBS. The brain was dissected and post-fixed in 4% PFA in PBS for 2 h at 4 °C. Coronal slices (50 μm) containing the substantia nigra were obtained with the Vibratome 1000 Plus sectioning system (3 M). Brain slices were washed three times in PBS for 10 min at RT, and blocked and permeabilized in 0.3 % Triton X-100 in PBS (T-PBS) supplemented with 5 % normal goat serum for 1 h at RT. Coronal slices were then incubated with the appropriate primary antibody in 0.3 % T-PBS with 1 % NGS o/n at 4 °C. Brain slices were washed three times in PBS for 10 min at RT and incubated with the appropriate Alexa Fluor®-conjugated secondary antibody in 0.3 % T-PBS with 1 % NGS for 2 h at RT. Nuclei were stained with the fluorescent dye 4′,6-diamidino-2-phenylindole (DAPI) at a concentration of 1:500,000 in PBS (Thermo Fischer). Finally, slices were mounted with Fluoromount mounting medium (Sigma-Aldrich) on Superfrost Plus glass slides (VWR International, Leuven, Belgium). Images were taken using an inverted LSM900 confocal microscope (Zeiss) with a 63× or 20× objective using the same settings/laser power.

2.16. Biochemistry

To purify a Triton-insoluble postsynaptic fraction (TIF) highly enriched in postsynaptic density proteins [33], striata were homogenized with a hand-held Teflon-glass potter at 4 °C in ice-cold buffer (pH 7.4) containing 0.32 M sucrose, 1 mM HEPES, 1 mM $MgCl_2$, 1 mM $NaHCO_3$ and 0.1 phenylmethanesulfonylfluoride supplemented with Complete™ protease inhibitor cocktail tablets (Roche Diagnostics) and phosSTOP™ phosphatase inhibitor (Roche Diagnostics). An aliquot of the homogenate was frozen at − 20 °C, while the rest of the sample was centrifuged at 1000 *g* for 5 min at 4 °C to remove nuclear contamination and white matter. The supernatant was collected and spun at 13,000 *g* for 15 min at 4 °C. The resulting pellet (P2-crude membrane fraction) was resuspended in Triton-KCl buffer (1 % Triton™ X-100 and 150 mM KCl) and, after 15 min incubation on ice, spun at 100,000 *g* for 1 h at 4 °C. The pellet (TIF) was resuspended in 20 mM HEPES buffer supplemented with Complete™ protease inhibitor cocktail tablets and stored at −80 °C. TIF and homogenate samples for immunoblotting analysis were denatured with Laemmli buffer and 10 min heating at 98 °C.

For co-immunoprecipitation assays, homogenate and P2 aliquots containing 150 μg and 50 μg of proteins, respectively, were incubated overnight at 4 °C with the primary antibody in RIA buffer containing 50 mM Tris HCl (pH 7.2), 150 mM NaCl, 1 % NP-40, 0.2 % sodium dodecyl sulfate (SDS), and 0.5 % deoxycholic acid. A control no-IgG sample was always prepared under the same conditions without the antibody. Protein A and G magnetic beads (SureBeads, Biorad) were washed three times in PBS-T (0.1 % Tween-20 in PBS), resuspended in RIA buffer, added to each sample, and incubated for 2 h on a wheel at RT. Beads were precipitated by quick centrifugation and washed three times in RIA buffer supplemented with 0.1 % SDS and boiled for 10 min in Laemmli

buffer. Beads were magnetized and the supernatant loaded in a proper acrylamide gel for SDS-PAGE, and interacting proteins were revealed by immunoblotting.

For Western blotting assays, the protein content of TIF and homogenate samples was quantified by Bradford assay. All samples were standardized at a concentration of 1 mg/ml and denatured chemically with Laemmli buffer and thermally by heating at 98 °C for 10 min. TIF and total homogenate proteins were separated with SDS-PAGE, followed by Western blotting analysis. A total of 10 − 15 μg of proteins were separated on 6–12 % acrylamide/bisacrylamide gel and transferred to a nitrocellulose membrane (Biorad). The membranes were then incubated for 1 h at RT in blocking solution (I-block, TBS 1X, and 20 % Tween-20) on a shaker, and then incubated with the specific primary antibody in blocking solution overnight at 4 °C. The following day, after three washes with TBS and Tween 20 (TBS and 0.1 % Tween20; TBSt), they were incubated with the corresponding horseradish peroxidase (HRP)-conjugated secondary antibody in blocking solution for 1 h at RT. After washing with TBSt, membranes were developed with electrochemiluminescence (ECL) reagents (Biorad). Finally, membranes were scanned with a Chemidoc (Biorad Universal Hood III) using Image Lab software (Biorad). Bands were quantified with computer-assisted imaging (Image Lab, Biorad). Protein levels were expressed as relative optical density (OD) measurements normalized to a housekeeping protein.

2.17. Antibodies

Rabbit anti-αsyn (D37A6) (WB 1:1000, Cell Signaling #4179); mouse anti-αsyn (WB 1:1000, ICC 1:200, BD #610 787); anti polyclonal Rph3A (WB 1:2000; ICC 1:300, Protein Tech #11396–1-AP); and rabbit anti-Rph3A (WB 1:1000, Synaptic System #118003). Rabbit anti-GAPDH (WB 1:5000, Santa Cruz #sc-25778). (Mouse anti-tubulin (WB 1:30000; #T9026, Sigma), rabbit anti-GluN2A (WB 1:1000, ICC 1:100, #M264, Sigma); rabbit anti-GluN2B (WB 1:1000, #718600, Invitrogen); mouse anti-GluN2D (WB:1:1000 #MAB5578, Millipore); Rabbit anti-GluA1 (WB 1:1000 #13185, Cell Signaling), rabbit monoclonal anti-phosphoSer845-GluA1 (WB 1:1000 #04–1073, Merck-Millipore); mouse anti-GluA2 (WB 1:1000 #75–002 Neuromab); and mouse anti-GluA3 (WB 1:1000 #MAB5416 Millipore). Rabbit anti tyrosine hydroxylase (WB 1:10000 #AB152 Millipore) Rat anti-Dopamine transporter (WB 1:1000, IHC 1:500 Sigma-Aldrich #MAB369**)**. Monoclonal anti-PSD-95 (WB 1:1000, #K28/43, Neuromab); and anti-tGFP ICC (1:300 #AB513, Evrogen). Polyclonal αsyn and phospho S129 (IHC 1:100, ab51253, Abcam).

2.18. Statistical analysis

Western blot quantification was performed with ImageLab software (Biorad). Protein levels were expressed as relative OD normalized on tubulin levels as housekeeping proteins.

Images acquired with a confocal microscope were analyzed with Fiji/Image J software. Statistical analysis was performed with GraphPad Prism 8 software and data were presented as mean ± SEM (standard error of the mean).

The tests used to assess data significance are indicated in the figure legends. In particular, the following tests were used, as appropriate: two-tailed unpaired Student's *t*-test, Mann–Whitney test, one-way ANOVA, or Kruskal–Wallis test.

The numbers of neurons and mice used are reported in the figure legends. For the confocal image analyses, at least 10 neurons from three different experiments were analyzed. For rotarod tests, the mean of three consecutive trials was used for analysis. For grip strength tests, the mean of the five values was considered for the analysis. Experimenters were not blinded during data acquisition, but all analyses were performed with blinding of the experimental conditions.

2.19. Availability of data and materials

The datasets used and/or analysed during the current study are available from the corresponding author on reasonable request.

3. Results

3.1. In vitro assessment of αsyn/Rph3A binding

We used different experimental approaches to confirm and characterize the αsyn/Rph3A interaction [23] in a physiological setting. Colocalization analysis of αsyn and Rph3A on primary hippocampal neurons at *days in vitro 16 (DIV16)* was performed with confocal microscopy combined with structured illumination microscopy (SIM), allowing an x-y resolution of about 100–110 nm [34]. As shown in Fig. 1A, several spots of Rph3A/αsyn colocalization were detected along dendrites of GFP-transfected neurons. A proximity ligation assay (PLA) was performed to further investigate the interaction of the two proteins.

This approach showed the presence of many PLA-positive signals when αsyn and Rph3A antibodies were used to label endogenous proteins (Fig. 1B), indicating that the two proteins are in proximity (<40 nm) to each other, as in a direct protein–protein complex. Interestingly, PLA clusters were not only present along neurites but also in proximity to the dendritic spines of GFP-transfected neurons. Finally, a biochemical approach was used to confirm the imaging data. Co-immunoprecipitation experiments were conducted on a total homogenate of rat forebrain and, considering αsyn and Rph3A's interplay with membranes, on the crude membrane fractions (P2). As shown in Fig. 1C, the αsyn/Rph3A protein complex was detected in both αsyn and Rph3A-immunoprecipitated samples.

3.2. In silico characterization of the αsyn/Rph3A binding mode

In silico structural analysis was employed to characterize the binding mode of the protein complex. The Rph3A C2B domain binds two Ca^{2+} ions and one IP_3 molecule and is homologous to the C2-like domains of synaptotagmin-1 and − 3, which are involved in interactions with SNAREs such as SNAP25 and Ca^{2+}-triggered exocytosis of synaptic vesicles [35,36]. Furthermore, SNAREs' conserved coiled structure is similar to the NMR structure of the non-fibrillary monomeric αsyn when bound to micelles (PDB: 1XQ8), suggesting that αsyn could bind similarly to the Rph3A C2B domain. Accordingly, the Rph3A C2B domain's primary and three-dimensional structures were analyzed, particularly their surface charges, starting from the available experimentally solved rat Rph3A structures. Notably, the primary structures of rat (P47709) and human (Q9Y2J0) Rph3A C2B domains (aa 550–683) match perfectly. This allowed us to build a homologous model of the human domain, using the crystallized C2B-domain rat structure as a template. Using the MOE suite, experimentally solved structures corresponding to rat Rph3A (2CM5, 5LOB, 5LOW, and 5LO8) were aligned. The reference structures for comparative modeling were selected according to their sequence coverage and the presence of Ca^{2+} ions (2CM5) and PIP2 (5LO8). The final model is shown in Fig. 2A (see Fig. S1 for detailed multiple-sequence alignment).

To identify a preferential binding surface for interaction with αsyn, a protein patch analysis was conducted on our model and the results were compared with the SNAP25 C2B binding surface [35]. Fig. 2B shows two α-helical regions located within the C2B bottom surface that have been identified as the amino acidic stretches that can potentially bind αsyn. Residues thought to be critical for the studied interaction are Ser618, Lys622, Lys623, Lys651, and Lys663.

3.3. In silico screening of libraries of commercial compounds

The identification of compounds that can uncouple the αsyn/Rph3A protein complex was used as a proof-of-concept of our hypothesis. The

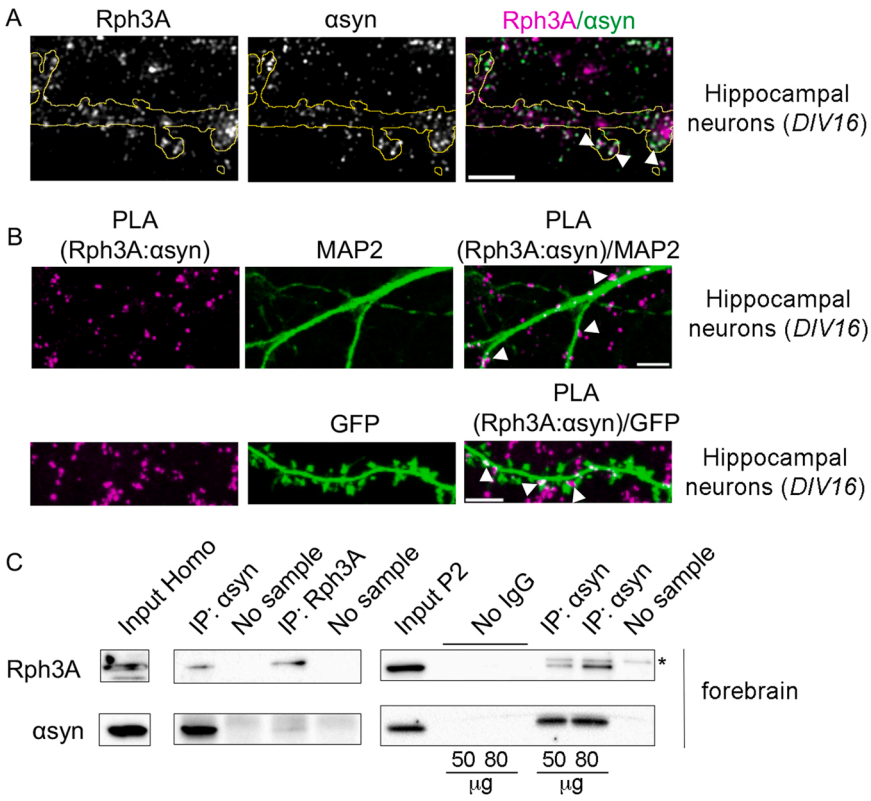

Fig. 1. *In vitro* assessment of Rph3A/αsyn binding. (A) Representative structured illumination microscopy (SIM) images of αsyn (green) and Rph3A (magenta) along dendrites of GFP-transfected (yellow mask) neurons in *DIV16* rat hippocampal neurons. Scale bar: 2 μm. (B) In situ detection of proximity ligation assay (PLA) of αsyn/Rph3A complexes (magenta) along MAP2-positive dendrites (green; upper panels) and GFP-transfected neurons (green; lower panels) of *DIV16* primary hippocampal cultures. Scale bar: 5 μm. (C) Co-immunoprecipitation analysis of αsyn/Rph3A complexes in homogenate (Homo - 150 μg) and crude membrane fraction (P2 - 50 μg, 80 μg) of adult rat forebrain (right), performed with protein A sepharose beads and protein A magnetic beads, respectively. *non-specific higher molecular weight band.

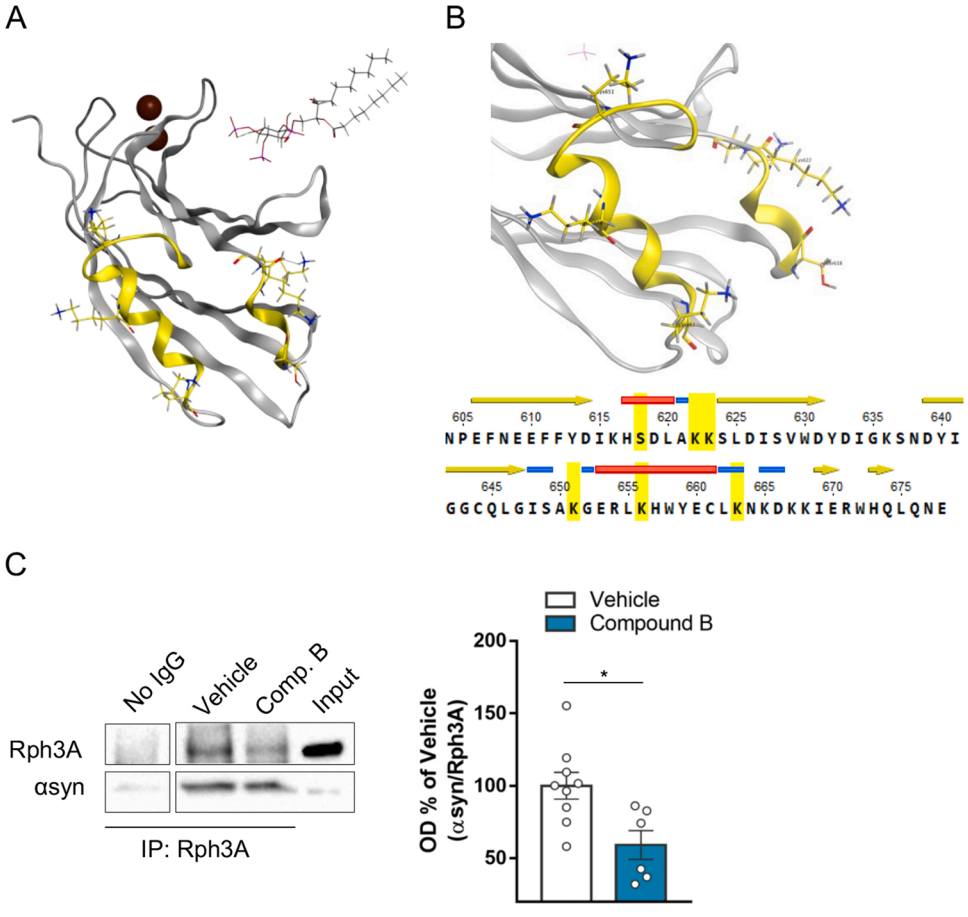

Fig. 2. *In silico* characterization of αsyn/Rph3A binding mode. (A) The C2B Rph3A homology model built with MOE showing Ca^{2+} ions, and PIP2 co-crystallized ligands. (B) Structure of the C2B bottom surface of Rph3A, showing the two α-helices (yellow) hypothesized to bind αsyn with the lateral chains of the target Lys651, Lys656, Lys663, Ser618, and Lys622 (highlighted in yellow in the reported protein sequence). Yellow arrows and red bars indicate organized β-sheet and α-helical regions, respectively. (C) Co-immunoprecipitation analysis of αsyn and Rph3A in corticostriatal slices treated with Compound B. Levels of αsyn were evaluated by WB analysis on Rph3A IP, normalized on the corresponding Rph3A band and expressed as % of optical density (OD) of the control mean. 15 % of the amount of homogenate used for co-IP analysis was loaded as input control. Vehicle, n = 9 rats; Compound B, n = 6 rats. Data information: in C data are presented as mean±SEM.*$P < 0.05$ (Student's *t*-test).

model of the Rph3A C2B-domain was selected to perform an *in silico* screening of libraries of commercially available compounds that can bind the target Rph3A region. The polybasic stretch of the amino acids Lys622, Lys623, Lys651, and Lys663 confers a positive charge to this region of Rph3A, a feature that was considered a fundamental constraint for the compound screening. The compounds evaluated as binders of the target Rph3A region and, consequently, able to interfere with the Rph3A/αsyn complex, were chosen from the *Asinex BioDesign* and *Asinex Gold & Platinum* libraries (see Materials and Methods).

Considering the structural and chemical properties of the target Rph3A surface and its basic nature, molecules were filtered to retain those bearing negative charges. Charge-related molecular descriptors were calculated with MOE, specifically, the total charge (Fcharge) and the number of acidic atoms (a_acid) displayed by the molecules. The compounds exceeding this selection constituted the final library, including 15,454 molecules that were used for the protein-ligand docking studies. An initial protein-peptide docking was performed with the Schrödinger's Glide software. From the results of the docking procedures, the 7 top-scoring molecules were selected according to both docking score and visual inspection, and subsequently subjected to a more accurate docking protocol, using the Glide extra precision (XP) mode. Most importantly, the final three compounds selected were chosen in part by a second visual inspection of the docking poses. This was necessary to eliminate compounds with a favorable docking score that did not bind to the selected Rph3A cleft. In parallel, protein-ligand docking analyses were performed on the library of acidic compounds as well, using the MOE software to select 19 promising molecules. With this strategy, we prioritized different parameters and scoring functions to increase the efficiency of the selection procedure.

Ligands interacting with at least one of Lys623, Lys651, Lys656, or Lys663 were used to create a final database. The database included 19 compounds from the MOE-based prioritization representing the top-scoring ligands among the compounds that could interact with Lys663, six compounds that could interact with both Lys663 and Lys623, and five compounds that could interact with Lys651 and Lys663. A final library of 22 molecules, including the 19 selected compounds from the MOE docking results and the three top-scoring ligands obtained with Glide XP docking were analyzed to predict their molecular properties and descriptors (physicochemical, pharmacokinetic, and toxicological) using the ACD/Percepta suite, to select candidate compounds that could be studied in an *in vitro* system. Moreover, for each compound, the central nervous system (CNS) activity, the ability to penetrate the blood–brain barrier (BBB), the logP (Octanol-water partition coefficient), and Lipinski's rule violations were calculated. Four compounds with different physicochemical properties were selected, considering the predicted properties, docking poses, and scores (see Table 1). To further validate the selection, these four compounds were then subjected to final docking analyses using MOE, confirming their binding ability as reported in Table 1.

These four selected molecules were then tested *ex-vivo* for their ability to modulate Rph3A/αsyn binding. To evaluate the candidate compounds' ability to disrupt the Rph3A/αsyn interaction, acute corticostriatal slices were treated with each compound (10 μM) or the vehicle solution. After incubation, striata were separated from the cortex and co-immunoprecipitation assays were performed from striatal lysates. As shown in Fig. 2C, Compound B led to a significant decrease in the amount of Rph3A bound to αsyn compared with control slices. No other compound altered the Rph3A/αsyn complex (Fig. S2).

3.4. Role of Rph3A/αsyn interaction in the αsyn-PFF in vitro neuronal model

To address the role of the Rph3A/αsyn complex in αsyn-mediated synaptic toxicity, we exploited a recently validated *in vitro* neuronal model of αsyn-induced spine pathology [37]. To do so, αsyn-PFF were prepared from purified monomeric αsyn (see Materials and Methods) [5,29] and analyzed through TEM before being used as previously reported [5]. EGFP-transfected primary hippocampal neurons were treated at *DIV9* with αsyn-PFF (1 and 2 μg/ml). As previously reported [37], spine morphology analysis revealed a significant dose-dependent reduction of dendritic spine density at *DIV16* (Fig. 3A), in absence of modifications in dendritic spine size or subtypes (see Fig. S3).

Considering the above-described αsyn/Rph3A complex (see Figs. 1–2) and the role of Rph3A in the synaptic stabilization of GluN2A-containing NMDARs in hippocampal neurons [15,16], we evaluated the effect of αsyn-PFF (2 μg/ml) on Rph3A synaptic levels and GluN2A surface levels. The confocal microscopy analysis in EGFP-transfected primary hippocampal neurons revealed that αsyn-PFF significantly decreased the percentage of Rph3A+ spines when compared with control neurons (Fig. 3B). In agreement with previous studies [15–17] the reduction of Rph3A postsynaptic localization was associated with a significant decrease in the levels of GluN2A-containing NMDARs on the cell surface (Fig. 3C). Since primary hippocampal neurons show high expression of GluN1/GluN2A/GluN2B tri-heteromeric NMDARs, we also assessed GluN2B surface levels, without finding any significant differences upon αsyn-PFF-treatment (Fig. 3D).

To assess the role of the Rph3A/αsyn complex in these events, we evaluated the effects of the Rph3A/αsyn uncoupling molecule in reversing αsyn-PFF-induced spine loss. Compound B (see Table 1) was administered at *DIV12*, concomitant with the beginning of αsyn-PFF neuropathology propagation [37]. Compound B did not modify the dendritic spine density of control-treated neurons (Fig. S4), but fully prevented the spine loss observed in αsyn-PFF-treated neurons (Fig. 4A).

As an alternative strategy to evaluate the role of Rph3A protein levels in αsyn-PFF-mediated synaptic toxicity, neurons were treated with αsyn-PFF at *DIV9* and co-transfected at *DIV11* with EGFP and a plasmid expressing fluorescently tagged Rph3A (RFP-Rph3A). Indeed, overexpression of Rph3A in primary hippocampal cultures was recently shown sufficient to increase dendritic spine density [17]. As a control, vehicle- and αsyn-PFF-injected neurons were co-transfected with the RFP tag. Similar to the results obtained with Compound B, the overexpression of RFP-Rph3A prevented the spine loss observed in neurons

Table 1
Table reporting the formal charge (FCharge), number of acidic group (a_acid), the docking score, CNS score, LogP and Lipinski violations of the selected Asinex compounds.

	FCharge	a_acid	Docking score (kcal/mol)	Rescoring (kcal/mol) MOE	CNS score	LogP	Lipinski violations
Compound A	-4	3	-6.1 (MOE)	-6.2	-2.85 (penetrant)	optimal	0
Compound B	-4	8	-3.8 (MAESTRO)	-7.4	-7.53 (non penetrant)	lipophilic	4
Compound C	-2	4	-5.0 (MAESTRO)	-7.2	-6.87 (non penetrant)	optimal	0
Compound D	-1	3	-5.7 (MOE)	-6.2	-3.30 (weak penetrant)	optimal	0

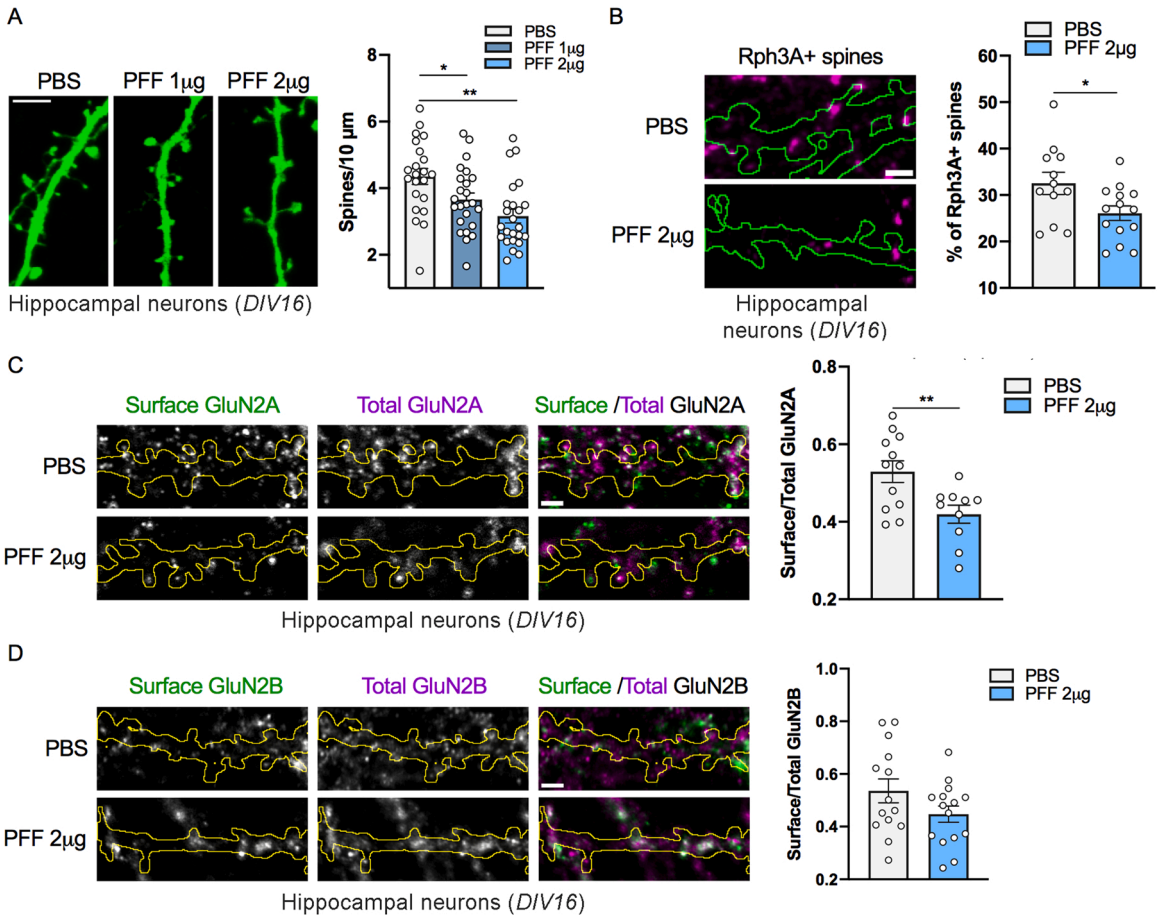

Fig. 3. Morphological and molecular effects induced by αsyn-PFF in primary hippocampal neurons. (A) Representative confocal images and quantification of spine density of EGFP-transfected hippocampal neurons upon 7-day treatment with αsyn-PFF (1 or 2 µg) or PBS. n = 24 neurons for each group. Scale bar: 3 µm. (B) Representative confocal images and bar graph showing the percentage of Rph3A-positive dendritic spines (of the total spines) in EGFP-transfected hippocampal neurons upon 7-day treatment with αsyn-PFF (2 µg) or PBS. scale bar, 2 µm. PBS, n = 12 neurons; PFF, n = 14 neurons. (C) Confocal images of surface (green) and total (magenta) GluN2A staining in EGFP-transfected neurons upon 7-day treatment with αsyn-PFF (2 µg) or PBS. Bar graph represents mean ± SEM of the GluN2A surface/total ratio of fluorescent intensity. Scale bar: 2 µm. PBS, n = 12 neurons; PFF, n = 10 neurons. (D) Confocal images of surface (green) and total (magenta) GluN2B staining in EGFP-transfected neurons upon 7-day treatment with αsyn-PFF (2 µg) or PBS. Bar graph represents mean ± SEM of the GluN2B surface/total ratio of fluorescent intensity. Scale bar: 2 µm. PBS, n = 14 neurons; PFF, n = 15 neurons. Data information: in (A) data are presented as mean±SEM. *P < 0.05 ***P < 0.0005 (Mann-Whitney test); in (B) data are presented as % of control mean±SEM; in (C), (D) data are presented as mean±SEM. *P < 0.05, **P < 0.05 (Student's *t*-test).

treated with αsyn-PFF (Fig. 4B).

3.5. Role of Rph3A/αsyn interaction in the αsyn-PFF in vivo neuronal model

We moved to investigate the role of Rph3A and the Rph3A/αsyn interplay in an early *in vivo* model of synucleinopathy. Rodent models are valid tools to reproduce early PD manifestations experimentally *in vivo* based on the injection of pre-formed toxic αsyn species such as αsyn-PFF. These *in vivo* models are characterized by a slow, progressive disease, allowing the investigation of mechanisms underlying pathology progression from the very early stages, such as early synaptic dysfunction [25,38]. To investigate the impact of pathologic αsyn-PFF on the corticostriatal glutamatergic synapse, we exploited the highly validated mice model generated by Luk and coworkers [25], in which normal striatal dopamine levels and limited αsyn pathology were found at 42 days post injection (dpi42) and significant dopaminergic neurodegeneration is reported at dpi120. Notably, at dpi84, αsyn-PFF alters synaptic plasticity in rodent models within the nigrostriatal circuits associated with early behavioral abnormalities [5]. However, the molecular and postsynaptic mechanisms by which αsyn affects synaptic architecture and activity specifically, finally causing dysfunction in the nigrostriatal and the glutamatergic cortico-striatal circuitry, remain elusive. Therefore, to investigate the precocious changes in αsyn-mediated synaptic dysfunction that precede neuronal death, analyses were focused on dpi42 and dpi84 (Fig. 5A). Initial analyses were performed at dpi84. At this time, striatal injection of αsyn-PFF led to the retrograde transmission of αsyn pathology to the SNpc, as indicated by perinuclear phosphor-Ser129-αsyn (p-αsyn) positive inclusions visible in dopamine transporter (DAT)-labeled dopaminergic neurons [5,25] (see Fig. S5). Importantly, at this stage, αsyn-PFF did not induce significant deterioration of dopaminergic striatal fibers as measured by the WB of the striatal and dopaminergic neuronal marker tyrosine hydroxylase (TH) and DAT [5,25] (Fig. S6). We then moved to evaluate αsyn-PFF-mediated synaptic toxicity. First, we focused on the molecular organization of the striatal excitatory post-synaptic compartment. Specifically, a subcellular fraction particularly enriched in proteins of excitatory postsynaptic density (Triton-insoluble fraction; TIF) was purified [33] to analyze the levels of ionotropic glutamate receptor subunits. Concurring with the simultaneous presence of significant alterations of cortico-striatal synaptic plasticity [5], αsyn-PFF mice at dpi84 displayed a profound alteration of the postsynaptic composition of the glutamatergic synapse. Specifically, mice were characterized by significantly reduced postsynaptic levels of the AMPAR subunit GluA1

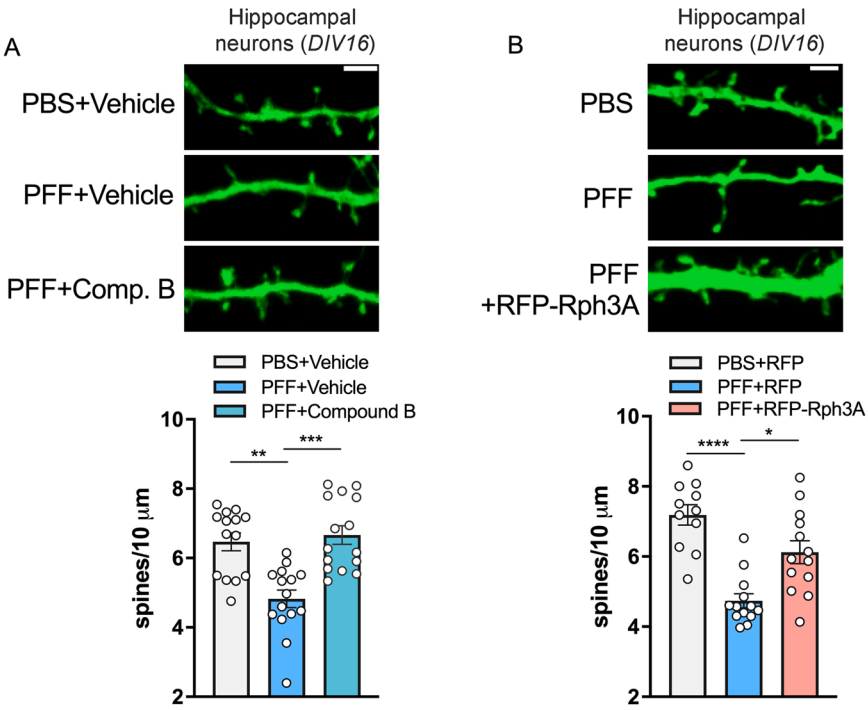

Fig. 4. Effects of Rph3A/αsyn uncoupling compound and Rph3A overexpression on αsyn-PFF-induced spine loss in primary hippocampal neurons. (A) Representative confocal images and quantification of spine density of hippocampal primary neurons transfected with GFP (green) upon 7-day αsyn-PFF (or PBS) treatment and co-administration of Rph3A/αsyn uncoupling compound (Compound B) or vehicle for the last 4 days. PBS+Vehicle, n = 14 neurons; PFF+Vehicle, PFF+Compound B, n = 15 neurons. Scale bar: 2 µm. (B) Representative confocal images and quantification of spine density of hippocampal primary neurons upon 7-day αsyn-PFF (or PBS) treatment and overexpression of RFP-Rph3A or RFP. PBS+RFP, n = 11 neurons; PFF+RFP, n = 13 neurons, PFF+RFP-Rph3A, n = 13 neurons. Scale bar: 2 µm. Data information: data are presented as mean±SEM. *P < 0.05, **P < 0.01, ***P < 0.001, ****P < 0.0001. (Kruskal-Wallis test followed by Dunn's *post hoc* test).

(Fig. 5B) and the NMDAR subunits GluN2A (Fig. 5C) compared with the controls. Although not statistically significant, the GluN2B subunit shows a decreasing trend upon treatment (Fig. 5B). Moreover, we observed also a significant reduction of the GluN2D subunit of the NMDAR, known to be enriched in striatal cholinergic interneurons [39], thus supporting the hypothesis that αsyn-PFF mice have at this stage an overall impairment of NMDARs at the postsynaptic membrane of both SPNs and interneurons. No alterations of the main PSD-protein PSD-95 were detected at this time at the synapses (Fig. 5C) or in striatal lysates (Fig. S7). Considering the above-described αsyn/Rph3A complex (see Figs. 1–2) and the role of Rph3A in the synaptic stabilization of GluN2A-containing NMDARs [15,16], we evaluated possible alterations of Rph3A synaptic levels and its interaction with GluN2A-containing NMDARs. As shown in Fig. 5D and E, injection of αsyn-PFF led to a significant reduction of both Rph3A levels and its binding to GluN2A at dpi84, presenting a molecular mechanism for the reduced presence of this NMDAR subunit at the synapses.

No effect of αsyn-PFF on total Rph3A levels in striatal lysates was observed (Fig. S7). Starting from the molecular impairments induced by αsyn-PFF (Fig. 5B-E) and published studies on functional alterations of synaptic plasticity [5], we investigated the impact of αsyn-PFF on SPN dendritic spine morphology at this time. *Ex-vivo* spine analysis revealed that αsyn-PFF injection significantly affected SPN spine density, causing a 25 % reduction compared with controls at dpi84 (Fig. 5F). In addition, the remaining spines show aberrantly increased spine head width (Fig. S8), leading to an increasing trend in the percentage of mushroom-shaped spines compared with controls. Conversely, no significant alteration of striatal synapses was observed at dpi42. The postsynaptic protein levels of AMPARs (GluA1, GluA2, and GluA3 subunits) and NMDARs (GluN2A, GluN2B, GluN2D) were unchanged in αsyn-PFF mice compared with control mice at dpi42 (Fig. 5G). Similarly, no alteration was observed in the postsynaptic levels of Rph3A and the main PSD-associated scaffolding element, PSD-95 (Fig. 5G).

Overall, these results indicate that *in vivo* injection of αsyn-PFF in mice induces a time-dependent reduction of Rph3A postsynaptic levels associated with decreased synaptic GluN2A- and GluN2D-NMDARs and GluA1-AMPARs and spine loss. As shown above, both Compound B (Fig. 4A) and Rph3A overexpression (Fig. 4B) mitigated αsyn-PFF-induced synaptic toxicity in the neuronal *in vitro* model. Accordingly, we evaluated whether the same experimental strategies were effective to counteract the detrimental effects of αsyn-PFF *in vivo*. The intrinsic physicochemical properties of Compound B, the molecule that can interfere with the αsyn/Rph3A complex (see Fig. 2C), could represent an obstacle for its crossing the blood–brain barrier, thus making the intracerebral delivery more appropriate. To attain adequate concentrations of Compound B in the central nervous system in a chronic experimental setting, mice were implanted with a guide cannula in the lateral cerebral ventricle. As shown in Fig. 6A, αsyn-PFF injected mice were treated with Compound B or the vehicle solution every 3 days for 2 weeks starting at dpi69. *Ex-vivo* spine morphology analysis demonstrated that administration of Compound B in αsyn-PFF mice fully reversed the SPN spine loss compared with vehicle-injected αsyn-PFF mice (Fig. 6B), confirming the molecule's efficacy in the *in vivo* model to counteract the deleterious effects of αsyn-PFF synaptic toxicity, as in primary neuronal cultures (Fig. 4A). To counteract αsyn-PFF-induced spine loss with Rph3A overexpression, an adeno-associated viral vector expressing GFP-Rph3A (AAV9-hSyn-GFP-Rph3A-WPRE) was stereotaxically injected into the dorsal striatum at dpi35 (see methods and Fig. S9 for coordinates). This timing allowed peak expression of the protein to be reached during the progression of the early disease stages, as verified by WB analysis (Fig. S10). An AAV expressing GFP was used as the control (Fig. 6C). Again, in agreement with *in vitro* results (Fig. 4B), striatal Rph3A overexpression fully recovered SPN spine density in αsyn-PFF-injected mice at dpi84 (Fig. 6D). Interestingly, Rph3A overexpression in the dorsal striatum of control mice did not induce any modification of SPN spine density, indicating a specific counteraction of αsyn-mediated spine loss (Fig. S11).

Studies on experimental rodent models indicate that injecting αsyn-PFF induces motor and behavioral impairments starting about 3 months after injection. However, some discrepancies in the type and subtype of behavioral alterations exist, mainly ascribable to differences in the animal model or strain of pathologic αsyn used and the use of a bilateral or unilateral injection [5,25,38]. In this study, mice were challenged at dpi75–84 with different motor behavior tests (Fig. 7). To evaluate the effect of pharmacological approaches targeting Rph3A on motor behavior, we focused on Rph3A overexpression to avoid confounding

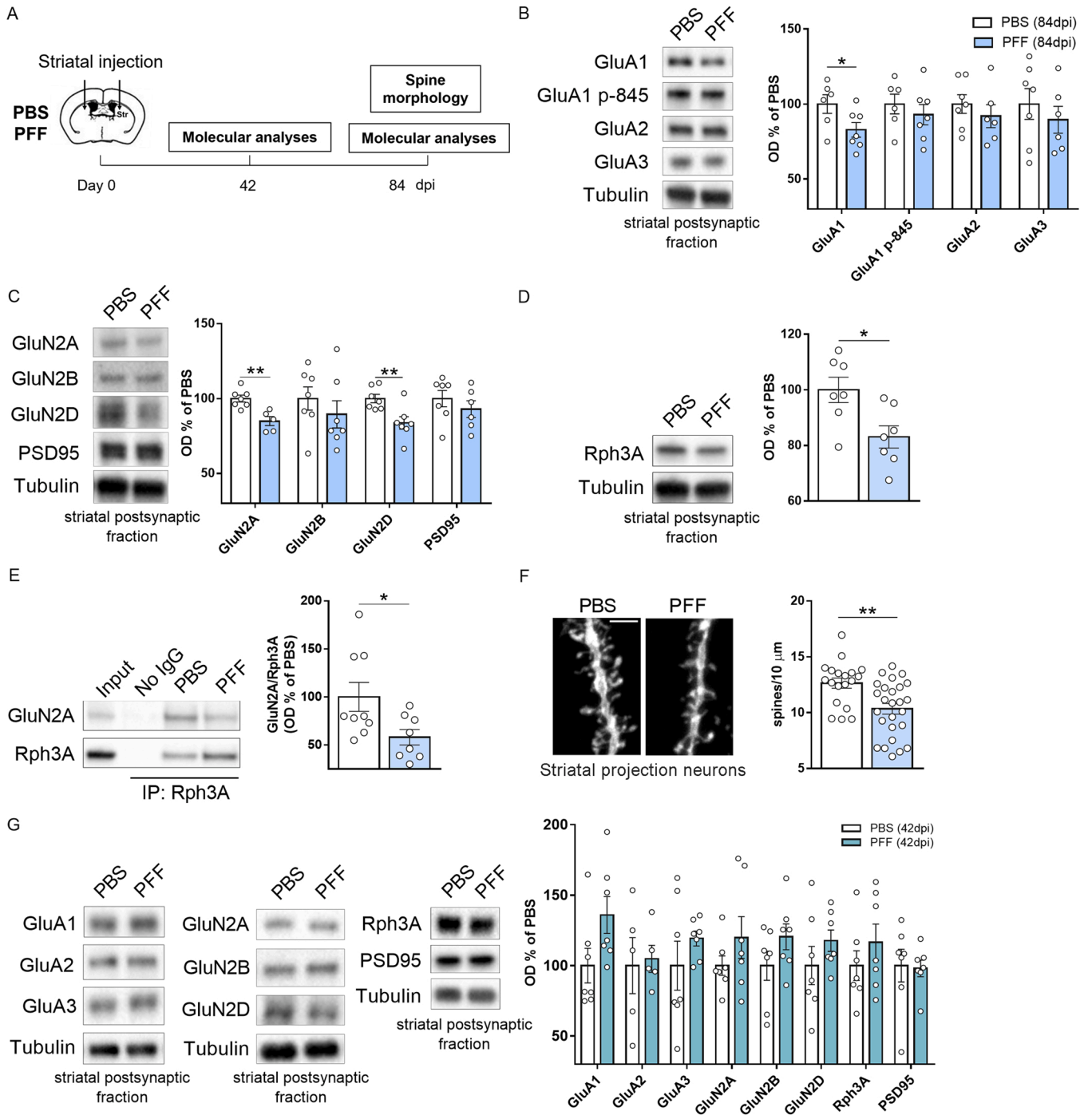

Fig. 5. Morphological and molecular effects induced by αsyn-PFF *in vivo* at striatal synapses. (A) Scheme representing the timeline of the experimental procedures. (B) Western blot representative images (left panels) and bar graph of densitometric quantification (right panels) of the AMPAR (GluA1, GluA1-p845, GluA2, and GluA3) subunits in striatal Triton-insoluble postsynaptic fractions (TIF) of αsyn-PFF and PBS-treated mice (dpi84). Protein levels were normalized on tubulin and reported as OD% of PBS-injected mice. PBS, n = 6–7 mice, PFF, n = 6–7 mice. (C)Western blot representative images (left panels) and bar graph of densitometric quantification (right panels) of the NMDAR (GluN2A, GluN2B, GluN2D) subunits and PSD-95 in striatal TIFs of αsyn-PFF and PBS-treated mice (dpi84). Protein levels were normalized on tubulin and reported as OD% of PBS-injected mice PBS. n = 7 mice, PFF, n = 5–6–7 mice. (D) Western blot representative images (left panels) and bar graph of densitometric quantification (right panels) of Rph3A in striatal TIFs of αsyn-PFF and PBS-treated mice (dpi84). Protein levels were normalized on tubulin and reported as OD% of PBS-injected mice. n = 7 mice for each group. (E) Western blot representative images (left panels) and bar graph of densitometric quantification (right panels) of GluN2A/Rph3A co-immunoprecipitation in homogenate fractions (150 µg) of αsyn-PFF and PBS-treated mice (dpi84). GluN2A protein levels were normalized on Rph3A and reported as OD% of PBS-injected mice. 15% of the amount of homogenate used for co-IP analysis was loaded as input control. PBS, n = 8 mice; PFF, n = 9 mice. (Mann–Whitney test). (F) Representative confocal images (left) and quantification of spine density in the striatum of αsyn-PFF and PBS-treated mice (dpi84). Scale bar: 3 µm. PBS, n = 19 neurons from 3 mice. PFF, n = 26 neurons from 3 mice. (G) Western blot representative images (left panels) and bar graph of densitometric quantification (right panels) of the AMPAR (GluA1, GluA2, and GluA3) and NMDAR (GluN2A, GluN2B, GluN2D) subunits and scaffolding proteins (Rph3A and PSD95) in striatal TIFs of αsyn-PFF and PBS-treated mice (dpi42). Protein levels were normalized on tubulin and reported as OD% of PBS-injected mice. n = 5–7 mice for each group. Data information: in (B-G) data are presented as mean±SEM. *P < 0.05, **P < 0.005 (Student's t-test; data with non-normal distribution were tested with Mann-Whitney test).

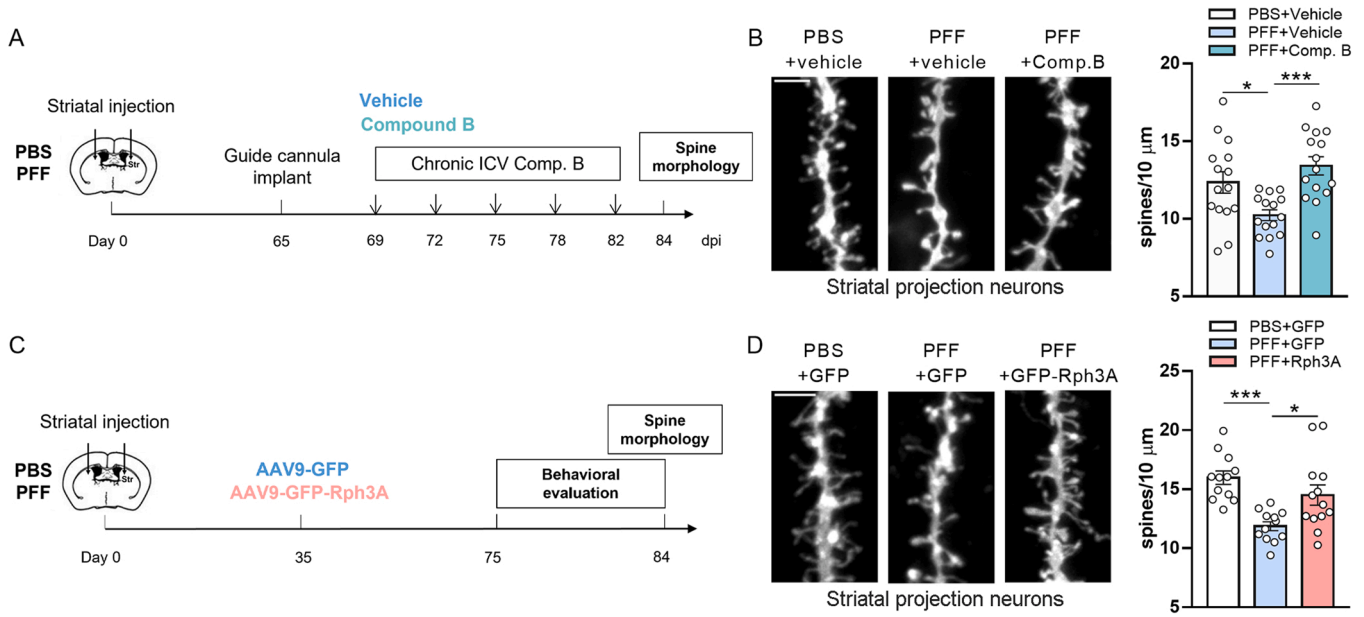

Fig. 6. *In vivo* effect of Rph3A/αsyn uncoupling compound and Rph3A overexpression on αsyn-PFF-induced spine loss in striatal neurons. (A) Scheme representing the timeline of the experimental procedures of the *in vivo* treatment with Compound B. (B) Representative images (left panels) showing dendrites of striatal neurons from mice treated with PBS, αsyn-PFF+vehicle, and αsyn-PFF+Compound B. Right panel: bar graph representing the dendritic spine densities in all experimental conditions. Scale bar = 3 µm. n = 15 neurons from 3 mice for each group. (C) Scheme representing the timeline of the experimental procedures of *in vivo* viral-mediated Rph3A overexpression in the striatum. (D) Representative images (left panels) showing dendrites of striatal neurons from mice treated with PBS, αsyn-PFF+GFP, and αsyn-PFF+GFP-Rph3A. Right panel: bar graph representing the dendritic spine densities in all experimental conditions. Scale bar = 3 µm. PBS+GFP, n = 12 neurons from 4 mice; PFF+GFP, n = 12 neurons from 4 mice; PFF+GFP-Rph3A, n = 13 neurons from 4 mice. Data information: in B, D data are presented as mean±SEM. *P < 0.05, ***P < 0.005 (one-way ANOVA followed by Tukey's *post hoc* test).

behavioral results associated to the chronic mice manipulation needed for compound B/vehicle injection through the intracerebral cannula.

First, mice were evaluated with the open field test to analyze their general locomotor ability and assess the presence of anxiety-like behavior. Specifically, locomotor activity was monitored for 10 min. As shown in Fig. 7A, no statistically significant alterations were found among PBS-GFP, αsyn-PFF-GFP, or αsyn-PFF-GFP-Rph3A mice in the distance traveled during the first and second 5-minute intervals of the task. Similarly, an analysis of the time the animals spent at the center and in the corners of the arena did not reveal any statistical differences among groups (Fig. 7B and C). These data indicate that at the time point considered, αsyn-PFF-lesions did not impair the general locomotor ability or spontaneous explorative and anxiety-like behaviors. Moreover, viral-mediated Rph3A overexpression in the striatum caused no effect on the open field tests (Fig. 7A-C).

Morphological results shown above indicate that both Compound B (Fig. 6A,B) and Rph3A overexpression (Fig. 6C,D) fully counteracted αsyn-PFF-induced spine loss in the mice model. To evaluate the effect of Rph3A striatal overexpression on motor behavior, rotarod and grip strength tests were performed to evaluate motor and coordination impairments more specifically. Mice were subjected at dpi75–84 to accelerated (20–40 rpm) and constant speed (30 rpm) rotarod tests (Fig. 7D and E). These motor behavior tests converged in identifying significant impairment of the motor coordination performances of αsyn-PFF mice compared with control animals. Notably, striatal delivery of AAV-GFP-Rph3A was sufficient to fully return αsyn-PFF mice's latency to fall from the rotarod to times comparable to those of control animals (Fig. 7D and E). Similarly, a significant decrease in forelimb muscle force in αsyn-PFF mice compared with control mice, as measured by the grip strength test, was fully recovered by striatal delivery of AAV-GFP-Rph3A (Fig. 7F). Overall, these data confirm the efficacy of Rph3A striatal overexpression as a strategy to counteract both spine loss and motor behavior deficits induced by αsyn-PFF.

4. Discussion

In the last 20 years, several studies investigated the role of the aggregation and toxicity of αsyn in the pathophysiology of familial and sporadic PD [40,41]. Aberrant forms and levels of αsyn can affect multiple cellular pathways and cause synaptic dysfunctions, resulting in the onset and progression of neurodegeneration. Although the precise mechanisms by which αsyn aggregates induce synaptic toxicity remain largely undescribed, αsyn's detrimental effects on synaptic function were reported in the early phases of the disease, long before the onset of significant dopaminergic neuronal loss [5,6,40–42].

Importantly, besides its presynaptic effect on the nigrostriatal dopaminergic system, toxic forms of αsyn also affect corticostriatal glutamatergic signaling, altering the postsynaptic activity of NMDARs both in PD [6] as well as in non-degenerative diseases such as dystonia [43]. In this study, we show that αsyn-PFF mice at dpi84 display significant loss of dendritic spines at striatal SPN associated with an impairment of the molecular composition of the postsynaptic glutamate receptor, consisting of a significant decrease in NMDAR-GluN2A and AMPAR-GluA1 subunits. Moreover, in line with previous literature findings [12] αsyn-PFF mice at dpi84 are characterized by a significant decrease of synaptic NMDAR-GluN2D, known to be enriched in striatal cholinergic interneurons [39]. No signs of neurodegeneration were detected at this time point. These data align with previous observations showing that both αsyn oligomers [6] and αsyn-PFF [5] interfere at early stages with LTP induction at SPN glutamatergic synapses. Conversely, here we show that αsyn-PFF-injected mice did not show significant alterations in ionotropic glutamate receptor levels at the striatal excitatory synapse at dpi42. This finding aligns with previous works showing normal striatal dopamine levels and limited αsyn pathology at dpi42 [25,38]. Finally, our study shows that αsyn-PFF induces a comparable toxic effect leading to spine loss and reduced NMDAR-GluN2A when used in a validated *in vitro* model of primary hippocampal neurons, thus suggesting a widespread toxicity of αsyn-PFF towards glutamatergic

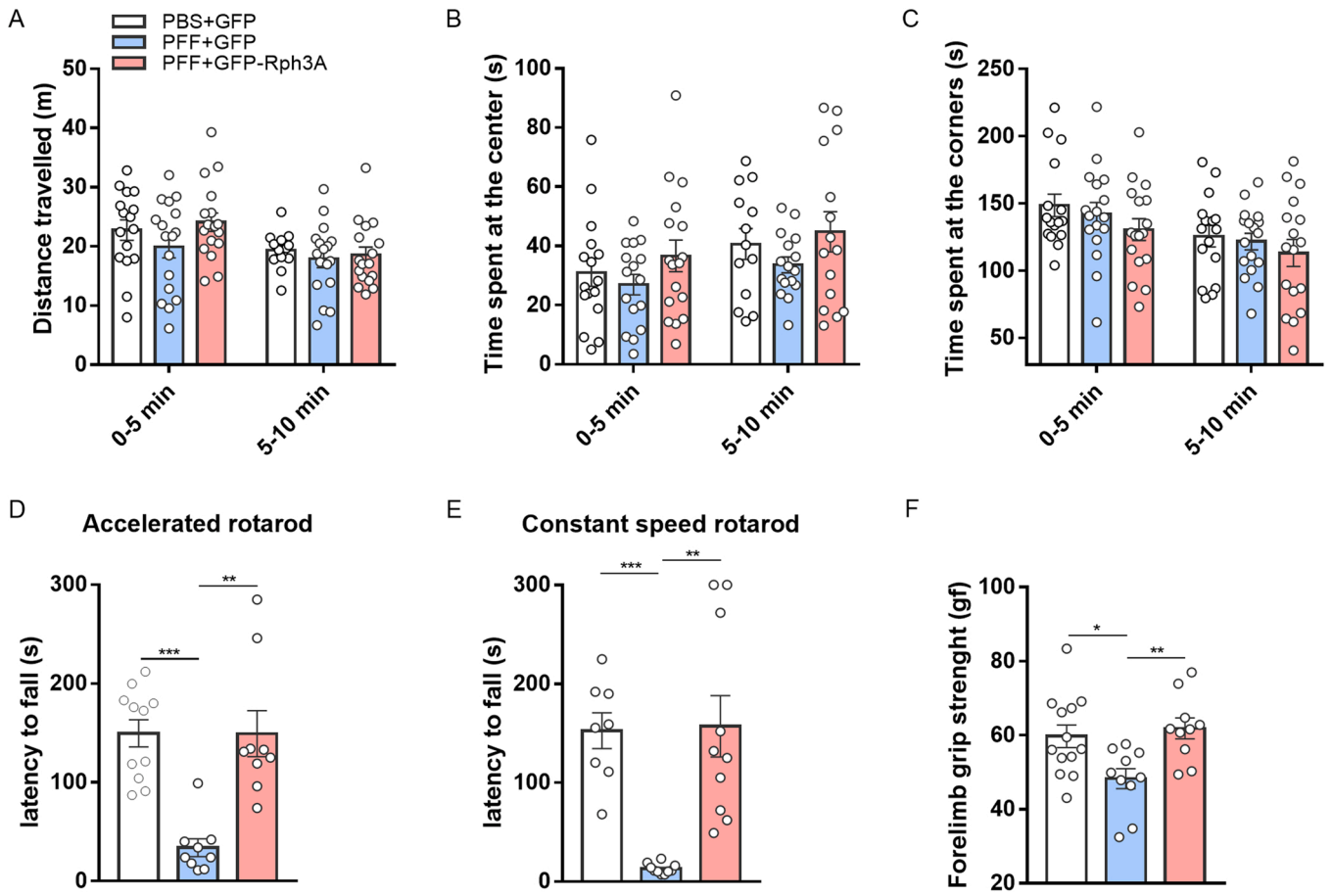

Fig. 7. Analysis of motor behavior of αsyn-PFF mice upon striatal delivery of GFP-Rph3A. (A) Distance traveled by PBS+GFP, αsyn-PFF+GFP, and αsyn-PFF+GFP-Rph3A mice evaluated in the Open field test. PBS+GFP, n = 15–16 mice; PFF+GFP, n = 16 mice, PFF+GFP-Rph3A, n = 15–17 mice. (B) Time spent at the center of the arena by PBS+GFP, αsyn-PFF+GFP, and αsyn-PFF+GFP-Rph3A mice evaluated in the Open field test. PBS+GFP, n = 13–16 mice; PFF+GFP, n = 16 mice, PFF+GFP-Rph3A, n = 15–17 mice. (C) Time spent at the corners of the arena by PBS+GFP, αsyn-PFF+GFP, and αsyn-PFF+GFP-Rph3A mice measured in the Open field test. PBS+GFP, n = 16 mice; PFF+GFP, n = 17 mice, PFF+GFP-Rph3A, n = 17 mice. (D) Accelerating rotarod performance (latency to fall in seconds) of PBS+GFP, αsyn-PFF+GFP, and αsyn-PFF+GFP-Rph3A mice. PBS+GFP, n = 11 mice; PFF+GFP, n = 9 mice, PFF+GFP-Rph3A, n = 9 mice. (E) Constant rotarod performance (latency to fall in seconds) of PBS+GFP, αsyn-PFF+GFP and αsyn-PFF+GFP-Rph3A mice. PBS+GFP, n = 8 mice; PFF+GFP, n = 10 mice, PFF+GFP-Rph3A, n = 10 mice. (F) Forelimb muscle strength measured by a grip strength meter. The force (*g*) exerted by each animal has been evaluated as the mean value of five consecutive trials. PBS+GFP, n = 13 mice; PFF+GFP, n = 10 mice, PFF+GFP-Rph3A, n = 10 mice. Data information: data are presented as mean±SEM. *P < 0.05, **P < 0.01, ***P < 0.001 (one-way ANOVA followed by Tukey's *post hoc* test; data with non-normal distribution were tested with Kruskal–Wallis followed by Dunn's multiple comparison test).

synapses enriched in GluN2A-containing NMDAs.

Our data demonstrate that αsyn-PFF induces a reduction of NMDAR synaptic levels without significantly altering the expression of NMDA in the total cell lysate, suggesting an augmented localization of NMDAR at extrasynaptic sites. These results are in line with very recent publications showing increased NMDAR extrasynaptic activity in the presence of αsyn aggregates [44] and, consequently, the neuroprotective effect of memantine [45], which is known to have preferential activity as an antagonist toward extrasynaptic receptors.

Altered levels of NMDARs and PSD-associated interacting proteins, including Rph3A, play a relevant role both in the pathophysiology of PD and in the onset of L-DOPA-induced motor complications [5,6,8,46]. Interestingly, previous findings indicated that Rph3A plays a key role in the aberrant synaptic localization of GluN2A-containing NMDARs in L-DOPA-induced dyskinesias. Specifically, interfering with the Rph3A/GluN2A complex at the synapse is sufficient to correct the aberrant synaptic localization of GluN2A-containing NMDARs in the rat model of dyskinesia [22,46]. In this study, starting from the characterization of a possible Rph3A/αsyn interaction [23], we moved to unravel Rph3A's possible role in the early phases of PD. αsyn-PFF mice at dpi84 displayed a selective reduction of postsynaptic Rph3A and its interaction with GluN2A in the absence of any change in total striatal levels of Rph3A. Considering Rph3A's key role in promoting the synaptic retention of GluN2A-containing NMDARs [15–17], these data offer a molecular explanation for the observed decrease in levels of this subunit at striatal synapses.

Our data also demonstrate that injection of αsyn-PFF leads also to a decreased postsynaptic localization of GluA1-containing AMPARs, thus indicating a generalized effect of the toxic aggregates on postsynaptic ionotropic glutamate receptors. Interestingly, these results are in line with a previous report showing that αsyn mutant forms can cause a decrease in AMPAR signaling *via* postsynaptic internalization of GluA1 subunits or inhibition of synaptic recruitment of these subunits [47]. Notably, these molecular impairments of the glutamatergic synapse were also reflected in morphological alterations of the dendritic spines of striatal SPNs. αsyn-PFF injection significantly reduced striatal spine density, indicating a precocious loss of synaptic contacts.

We used a bioinformatics approach that allowed us to identify the Rph3A C2B as the domain involved in αsyn binding. This Rph3A region had been shown to be involved in the interaction with the SNARE protein SNAP25, which shares structural similarity with αsyn [35]. A molecule (Compound B) that could target the identified C2B region,

selected *via* bioinformatic screening, was able to interfere with the formation of the Rph3A/αsyn complex, confirming the initial hypothesis. Data obtained from the *in vivo* model suggest that αsyn-PFF could promote mechanisms that can sequester Rph3A from physiological synaptic activities involving NMDARs. Interestingly, experimental strategies intended to reduce Rph3A postsynaptic activity had already proven to decrease not only the synaptic availability of GluN2A-containing NMDA receptors but also the spine density in hippocampal neurons [16]. Accordingly, treatment with Compound B or viral-mediated overexpression of Rph3A was able to fully prevent the loss of dendritic spines induced by αsyn-PFF in both the *in vivo* model's striatum and *in vitro* in primary hippocampal neurons. However, it is worth mentioning that the physicochemical structure of Compound B prevents systemic delivery, making this compound a poor drug candidate molecule. Therefore, Compound B can be considered a lead compound to be optimized using bioinformatics and chemical structural improvements before proceeding with the *in vivo* assessment of the efficacy of this Rph3A/αsyn uncoupling strategy.

Although some discrepancies have been reported, studies performed in transmissible αsyn rodent models indicate that motor impairments appear about 3 months after the lesions [5,6,25]. In this study, we detected reduced rotarod performance and decreased forelimb grip strength in αsyn-PFF mice at dpi84. The bilateral αsyn-PFF-injection can explain the more evident motor impairment found in this study compared with the milder dysfunctions previously reported in unilaterally-lesioned mice [25]. Bilateral lesions were recently reported to produce similar early behavioral defects in rats [5]. As general exploratory behavior evaluated in the open field test was not altered, it can be supposed that at this time, only more demanding motor tasks are affected [25]. Importantly, we demonstrated that striatal delivery of an AAV-Rph3A was able to fully repair the motor impairments observed in αsyn-PFF mice. This recovery of motor performances suggests that Rph3A striatal overexpression positively affects the overall nigrostriatal and cortico-striatal network, counteracting the detrimental effects of αsyn that lead to precocious motor impairments.

5. Conclusions

Among multiple mechanisms contributing to the pathology of PD, the accumulation of misfolded and toxic αsyn aggregates plays a well-demonstrated key role. In addition, accumulating evidence put forward the involvement in disease progression of other multiple factors such as inflammatory events, oxidative stress and mitochondria dysfunctions [48]. It's known that pathologic αsyn forms affect synaptic functions and structure before causing significant neurodegeneration. Here, we described the role of Rph3A as a novel mediator of early αsyn-PFF induced dendritic spines loss. Using *in vitro* and *in silico* approaches, we showed that Rph3A interacts with αsyn and we identified a small molecule able to interfere with the formation of this protein complex. Notably, interfering with Rph3A/αsyn complex or overexpressing Rph3A in the striatum were sufficient to prevent dendritic spine loss and motor defects in αsyn-PFF mice. Interestingly, Rph3A modulatory approaches also prevented synaptic loss in hippocampal primary neurons seeded with PFFs. Overall, rescue of Rph3A synaptic levels and activity can represent a novel experimental approach to counteract αsyn-PFF induced-postsynaptic dysfunction and early motor defects.

Funding

This work was supported by grants from Ministero dell'Istruzione, dell'Universita` e della Ricerca (MIUR) - PRIN (Bando 2017, Prot. 2017ENN4FY, F.G; Bando 2015, Prot. 2015FNWP34, F.G.).

CRediT authorship contribution statement

Elena Ferrari: Investigation, Formal analysis, Writing – original draft, Data curation, Visualization, Methodology. **Diego Scheggia:** Conceptualization, Methodology, Data curation, Writing – review & editinga. **Elisa Zianni:** Investigation, Methodology. Maria Italia: Investigation, Methodology. **Marta Brumana:** Investigation, Formal analysis. **Luca Palazzolo:** Investigation, Methodology, Writing – review & editing. **Chiara Parravicini:** Investigation, Writing – original draft. **Andrea Pilotto:** Conceptualization, Methodology. **Alessandro Padovani:** Conceptualization, Methodology. **Elena Marcello:** Conceptualization, Methodology, Writing – review & editing. **Ivano Eberini:** Supervision, Data curation, Formal analysis. **Paolo Calabresi:** Conceptualization, Methodology, Writing – review & editing. **Monica Diluca:** Conceptualization, Supervision, Writing – review & editing. **Fabrizio Gardoni:** Conceptualization, Data curation, Formal analysis, Supervision, Funding acquisition, Writing – original draft, Project administration, Writing – review & editing.

Conflicts of interest

The authors declare no conflict of interest.

Data availability

Data will be made available on request.

Acknowledgments

The authors thank Anna Grassi, and Ilaria Colombini for their excellent practical work. Part of this work was conducted at NOLIMITS, an advanced imaging facility established by the University of Milan.

Appendix A. Supporting information

Supplementary data associated with this article can be found in the online version at doi:10.1016/j.phrs.2022.106375.

References

[1] J.A. Obeso, M. Stamelou, C.G. Goetz, W. Poewe, A.E. Lang, D. Weintraub, D. Burn, G.M. Halliday, E. Bezard, S. Przedborski, S. Lehericy, D.J. Brooks, J.C. Rothwell, M. Hallett, M.R. DeLong, C. Marras, C.M. Tanner, G.W. Ross, J.W. Langston, C. Klein, V. Bonifati, J. Jankovic, A.M. Lozano, G. Deuschl, H. Bergman, E. Tolosa, E. Rodriguez-Violante, S. Fahn, R.B. Postuma, D. Berg, K. Marek, D.G. Standaert, D. J. Surmeier, C.W. Olanow, J.H. Kordower, P. Calabresi, A.H.V. Schapira, A. J. Stoessl, Past, present, and future of Parkinson's disease: A special essay on the 200th Anniversary of the Shaking Palsy, Mov Disord. 32 (2017) 1264–1310, https://doi.org/10.1002/mds.27115.

[2] M.G. Spillantini, M.L. Schmidt, V.M.-Y. Lee, J.Q. Trojanowski, R. Jakes, M. Goedert, α-synuclein in Lewy bodies, Nature 388 (1997) 839–840, https://doi.org/10.1038/42166.

[3] L. Xu, J. Pu, Alpha-synuclein in Parkinson's disease: from pathogenetic dysfunction to potential clinical application, Parkinson's Dis. 2016 (2016) 1–10, https://doi.org/10.1155/2016/1720621.

[4] B.A. Hijaz, L.A. Volpicelli-Daley, Initiation and propagation of α-synuclein aggregation in the nervous system, Mol. Neurodegener. 15 (2020) 19, https://doi.org/10.1186/s13024-020-00368-6.

[5] A. Tozzi, M. Sciaccaluga, V. Loffredo, A. Megaro, A. Ledonne, A. Cardinale, M. Federici, L. Bellingacci, S. Paciotti, E. Ferrari, A. La Rocca, A. Martini, N. B. Mercuri, F. Gardoni, B. Picconi, V. Ghiglieri, E. De Leonibus, P. Calabresi, Dopamine-dependent early synaptic and motor dysfunctions induced by α-synuclein in the nigrostriatal circuit, Brain (2021), awab242, https://doi.org/10.1093/brain/awab242.

[6] V. Durante, A. de Iure, V. Loffredo, N. Vaikath, M. De Risi, S. Paciotti, A. Quiroga-Varela, D. Chiasserini, M. Mellone, P. Mazzocchetti, V. Calabrese, F. Campanelli, A. Mechelli, M. Di Filippo, V. Ghiglieri, B. Picconi, O.M. El-Agnaf, E. De Leonibus, F. Gardoni, A. Tozzi, P. Calabresi, Alpha-synuclein targets GluN2A NMDA receptor subunit causing striatal synaptic dysfunction and visuospatial memory alteration, Brain 142 (2019) 1365–1385, https://doi.org/10.1093/brain/awz065.

[7] M.J. Diogenes, R.B. Dias, D.M. Rombo, H. Vicente Miranda, F. Maiolino, P. Guerreiro, T. Nasstrom, H.G. Franquelim, L.M.A. Oliveira, M.A.R.B. Castanho, L. Lannfelt, J. Bergstrom, M. Ingelsson, A. Quintas, A.M. Sebastiao, L.V. Lopes, T. F. Outeiro, Extracellular alpha-synuclein oligomers modulate synaptic transmission

and impair LTP via NMDA-receptor activation, J. Neurosci. 32 (2012) 11750–11762, https://doi.org/10.1523/JNEUROSCI.0234-12.2012.
[8] Y. Chen, W. Yang, X. Li, X. Li, H. Yang, Z. Xu, S. Yu, α-synuclein-induced internalization of NMDA receptors in hippocampal neurons is associated with reduced inward current and Ca2+ influx upon NMDA stimulation, Neuroscience 300 (2015) 297–306, https://doi.org/10.1016/j.neuroscience.2015.05.035.
[9] W. Yu, W. Yang, X. Li, X. Li, S. Yu, Alpha-synuclein oligomerization increases its effect on promoting NMDA receptor internalization, Int. J. Clin. Exp. Pathol. 12 (2019) 87–100.
[10] F. Cheng, X. Li, Y. Li, C. Wang, T. Wang, G. Liu, A. Baskys, K. Uéda, P. Chan, S. Yu, α-Synuclein promotes clathrin-mediated NMDA receptor endocytosis and attenuates NMDA-induced dopaminergic cell death: α-Synuclein promotes NMDA receptor endocytosis, J. Neurochem. 119 (2011) 815–825, https://doi.org/10.1111/j.1471-4159.2011.07460.x.
[11] L. Navarria, M. Zaltieri, F. Longhena, M.G. Spillantini, C. Missale, P. Spano, A. Bellucci, Alpha-synuclein modulates NR2B-containing NMDA receptors and decreases their levels after rotenone exposure, Neurochem. Int. 85-86 (2015) 14–23, https://doi.org/10.1016/j.neuint.2015.03.008.
[12] A. Tozzi, A. de Iure, V. Bagetta, M. Tantucci, V. Durante, A. Quiroga-Varela, C. Costa, M. Di Filippo, V. Ghiglieri, E.C. Latagliata, M. Wegrzynowicz, M. Decressac, C. Giampà, J.W. Dalley, J. Xia, F. Gardoni, M. Mellone, O.M. El-Agnaf, M.T. Ardah, S. Puglisi-Allegra, A. Björklund, M.G. Spillantini, B. Picconi, P. Calabresi, Alpha-synuclein produces early behavioral alterations via striatal cholinergic synaptic dysfunction by interacting with GluN2D N -methyl-D-aspartate receptor subunit, Biol. Psychiatry 79 (2016) 402–414, https://doi.org/10.1016/j.biopsych.2015.08.013.
[13] M.E. Burns, T. Sasaki, Y. Takai, G.J. Augustine, Rabphilin-3A: a multifunctional regulator of synaptic vesicle traffic, J. Gen. Physiol. 111 (1998) 243–255, https://doi.org/10.1085/jgp.111.2.243.
[14] Q. Bourgeois-Jaarsma, P. Miaja Hernandez, A.J. Groffen, Ca2+ sensor proteins in spontaneous release and synaptic plasticity: limited contribution of Doc2c, rabphilin-3a and synaptotagmin 7 in hippocampal glutamatergic neurons, Mol. Cell. Neurosci. 112 (2021), 103613, https://doi.org/10.1016/j.mcn.2021.103613.
[15] L. Franchini, J. Stanic, L. Ponzoni, M. Mellone, N. Carrano, S. Musardo, E. Zianni, G. Olivero, E. Marcello, A. Pittaluga, M. Sala, C. Bellone, C. Racca, M. Di Luca, F. Gardoni, Linking NMDA receptor synaptic retention to synaptic plasticity and cognition, IScience 19 (2019) 927–939, https://doi.org/10.1016/j.isci.2019.08.036.
[16] J. Stanic, M. Carta, I. Eberini, S. Pelucchi, E. Marcello, A.A. Genazzani, C. Racca, C. Mulle, M. Di Luca, F. Gardoni, Rabphilin 3A retains NMDA receptors at synaptic sites through interaction with GluN2A/PSD-95 complex, Nat. Commun. 6 (2015) 10181, https://doi.org/10.1038/ncomms10181.
[17] L. Franchini, J. Stanic, M. Barzasi, E. Zianni, D. Mauceri, M. Diluca, F. Gardoni, Rabphilin-3A drives structural modifications of dendritic spines induced by long-term potentiation, Cells 11 (2022) 1616, https://doi.org/10.3390/cells11101616.
[18] L. Yu, S. Tasaki, J.A. Schneider, K. Arfanakis, D.M. Duong, A.P. Wingo, T.S. Wingo, N. Kearns, G.R.J. Thatcher, N.T. Seyfried, A.I. Levey, P.L. De Jager, D.A. Bennett, Cortical proteins associated with cognitive resilience in community-dwelling older persons, JAMA Psychiatry 77 (2020) 1172, https://doi.org/10.1001/jamapsychiatry.2020.1807.
[19] R. Smith, Å. Petersén, G.P. Bates, P. Brundin, J.-Y. Li, Depletion of rabphilin 3A in a transgenic mouse model (R6/1) of Huntington's disease, a possible culprit in synaptic dysfunction, Neurobiol. Dis. 20 (2005) 673–684, https://doi.org/10.1016/j.nbd.2005.05.008.
[20] R. Smith, P. Klein, Y. Koc-Schmitz, H.J. Waldvogel, R.L.M. Faull, P. Brundin, M. Plomann, J.-Y. Li, Loss of SNAP-25 and rabphilin 3a in sensory-motor cortex in Huntington?s disease, J. Neurochem. 0 (2007), https://doi.org/10.1111/j.1471-4159.2007.04703.x.
[21] M.G.K. Tan, C. Lee, J.H. Lee, P.T. Francis, R.J. Williams, M.J. Ramírez, C.P. Chen, P.T.-H. Wong, M.K.P. Lai, Decreased rabphilin 3A immunoreactivity in Alzheimer's disease is associated with Aβ burden, Neurochem. Int. 64 (2014) 29–36, https://doi.org/10.1016/j.neuint.2013.10.013.
[22] J. Stanic, M. Mellone, F. Napolitano, C. Racca, E. Zianni, D. Minocci, V. Ghiglieri, M.-L. Thiolat, Q. Li, A. Longhi, A. De Rosa, B. Picconi, E. Bezard, P. Calabresi, M. Di Luca, A. Usiello, F. Gardoni, Rabphilin 3A: a novel target for the treatment of levodopa-induced dyskinesias, Neurobiol. Dis. 108 (2017) 54–64, https://doi.org/10.1016/j.nbd.2017.08.001.
[23] E. Dalfó, M. Barrachina, J.L. Rosa, S. Ambrosio, I. Ferrer, Abnormal α-synuclein interactions with rab3a and rabphilin in diffuse Lewy body disease, Neurobiol. Dis. 16 (2004) 92–97, https://doi.org/10.1016/j.nbd.2004.01.001.
[24] C.Y. Chung, J.B. Koprich, H. Siddiqi, O. Isacson, Dynamic changes in presynaptic and axonal transport proteins combined with striatal neuroinflammation precede dopaminergic neuronal loss in a rat model of AAV -synucleinopathy, J. Neurosci. 29 (2009) 3365–3373, https://doi.org/10.1523/JNEUROSCI.5427-08.2009.
[25] K.C. Luk, V. Kehm, J. Carroll, B. Zhang, P. O'Brien, J.Q. Trojanowski, V.M.-Y. Lee, Pathological α-synuclein transmission initiates Parkinson-like neurodegeneration in nontransgenic mice, Science 338 (2012) 949–953, https://doi.org/10.1126/science.1227157.
[26] I. Eberini, S. Daniele, C. Parravicini, C. Sensi, M.L. Trincavelli, C. Martini, M. P. Abbracchio, In silico identification of new ligands for GPR17: a promising therapeutic target for neurodegenerative diseases, J. Comput. Aided Mol. Des. 25 (2011) 743–752, https://doi.org/10.1007/s10822-011-9455-8.
[27] R.A. Friesner, J.L. Banks, R.B. Murphy, T.A. Halgren, J.J. Klicic, D.T. Mainz, M. P. Repasky, E.H. Knoll, M. Shelley, J.K. Perry, D.E. Shaw, P. Francis, P.S. Shenkin, Glide: a new approach for rapid, accurate docking and scoring. 1. Method and assessment of docking accuracy, J. Med. Chem. 47 (2004) 1739–1749, https://doi.org/10.1021/jm0306430.
[28] E. Harder, W. Damm, J. Maple, C. Wu, M. Reboul, J.Y. Xiang, L. Wang, D. Lupyan, M.K. Dahlgren, J.L. Knight, J.W. Kaus, D.S. Cerutti, G. Krilov, W.L. Jorgensen, R. Abel, R.A. Friesner, OPLS3: a force field providing broad coverage of drug-like small molecules and proteins, J. Chem. Theory Comput. 12 (2016) 281–296, https://doi.org/10.1021/acs.jctc.5b00864.
[29] N.K. Polinski, L.A. Volpicelli-Daley, C.E. Sortwell, K.C. Luk, N. Cremades, L. M. Gottler, J. Froula, M.F. Duffy, V.M.Y. Lee, T.N. Martinez, K.D. Dave, Best practices for generating and using alpha-synuclein pre-formed fibrils to model Parkinson's disease in rodents, JPD 8 (2018) 303–322, https://doi.org/10.3233/JPD-171248.
[30] R.A. Rudick, D.K. Zirretta, R.M. Herndon, Clearance of albumin from mouse subarachnoid space: a measure of CSF bulk flow, J. Neurosci. Methods 6 (1982) 253–259, https://doi.org/10.1016/0165-0270(82)90088-7.
[31] Y. Dai, N.L. Dudek, Q. Li, S.C. Fowler, N.A. Muma, Striatal expression of a calmodulin fragment improved motor function, weight loss, and neuropathology in the R6/2 mouse model of Huntington's disease, J. Neurosci. 29 (2009) 11550–11559, https://doi.org/10.1523/JNEUROSCI.3307-09.2009.
[32] G. Piccoli, C. Verpelli, N. Tonna, S. Romorini, M. Alessio, A.C. Nairn, A. Bachi, C. Sala, Proteomic analysis of activity-dependent synaptic plasticity in hippocampal neurons, J. Proteome Res. 6 (2007) 3203–3215, https://doi.org/10.1021/pr0701308.
[33] F. Gardoni, L.H. Schrama, A. Kamal, W.H. Gispen, F. Cattabeni, M. Di Luca, Hippocampal synaptic plasticity involves competition between Ca $^{2+}$ /calmodulin-dependent protein kinase II and postsynaptic density 95 for binding to the NR2A subunit of the NMDA receptor, J. Neurosci. 21 (2001) 1501–1509, https://doi.org/10.1523/JNEUROSCI.21-05-01501.2001.
[34] S. Hong, D.K. Wilton, B. Stevens, D.S. Richardson, Structured illumination microscopy for the investigation of synaptic structure and function, in: A. Poulopoulos (Ed.), Synapse Development, Springer New York, New York, NY, 2017, pp. 155–167. https://doi.org/10.1007/978-1-4939-6688-2_12.
[35] C. Ferrer-Orta, M.D. Pérez-Sánchez, T. Coronado-Parra, C. Silva, D. López-Martínez, J. Baltanás-Copado, J.C. Gómez-Fernández, S. Corbalán-García, N. Verdaguer, Structural characterization of the Rabphilin-3A–SNAP25 interaction, Proc. Natl. Acad. Sci. USA 114 (2017) E5343–E5351, https://doi.org/10.1073/pnas.1702542114.
[36] Q. Zhou, Y. Lai, T. Bacaj, M. Zhao, A.Y. Lyubimov, M. Uervirojnangkoorn, O. B. Zeldin, A.S. Brewster, N.K. Sauter, A.E. Cohen, S.M. Soltis, R. Alonso-Mori, M. Chollet, H.T. Lemke, R.A. Pfuetzner, U.B. Choi, W.I. Weis, J. Diao, T.C. Südhof, A.T. Brunger, Architecture of the synaptotagmin–SNARE machinery for neuronal exocytosis, Nature 525 (2015) 62–67, https://doi.org/10.1038/nature14975.
[37] Q. Wu, H. Takano, D.M. Riddle, J.Q. Trojanowski, D.A. Coulter, V.M.-Y. Lee, α-synuclein (αSyn) preformed fibrils induce endogenous αSyn aggregation, compromise synaptic activity and enhance synapse loss in cultured excitatory hippocampal neurons, J. Neurosci. 39 (2019) 5080–5094, https://doi.org/10.1523/JNEUROSCI.0060-19.2019.
[38] J.R. Patterson, M.F. Duffy, C.J. Kemp, J.W. Howe, T.J. Collier, A.C. Stoll, K. M. Miller, P. Patel, N. Levine, D.J. Moore, K.C. Luk, S.M. Fleming, N.M. Kanaan, K. L. Paumier, O.M.A. El-Agnaf, C.E. Sortwell, Time course and magnitude of alpha-synuclein inclusion formation and nigrostriatal degeneration in the rat model of synucleinopathy triggered by intrastriatal α-synuclein preformed fibrils, Neurobiol. Dis. 130 (2019), 104525, https://doi.org/10.1016/j.nbd.2019.104525.
[39] M. Mellone, E. Zianni, J. Stanic, F. Campanelli, G. Marino, V. Ghiglieri, A. Longhi, M.-L. Thiolat, Q. Li, P. Calabresi, E. Bezard, B. Picconi, M. Di Luca, F. Gardoni, NMDA receptor GluN2D subunit participates to levodopa-induced dyskinesia pathophysiology, Neurobiol. Dis. 121 (2019) 338–349, https://doi.org/10.1016/j.nbd.2018.09.021.
[40] Y.C. Wong, D. Krainc, α-synuclein toxicity in neurodegeneration: mechanism and therapeutic strategies, Nat. Med. 23 (2017) 1–13, https://doi.org/10.1038/nm.4269.
[41] J.C. Bridi, F. Hirth, Mechanisms of α-synuclein induced synaptopathy in Parkinson's disease, Front. Neurosci. 12 (2018) 80, https://doi.org/10.3389/fnins.2018.00080.
[42] F. Longhena, G. Faustini, M.G. Spillantini, A. Bellucci, Living in promiscuity: the multiple partners of alpha-synuclein at the synapse in physiology and pathology, IJMS 20 (2019) 141, https://doi.org/10.3390/ijms20010141.
[43] G. Ponterio, G. Faustini, I. El Atiallah, G. Sciamanna, M. Meringolo, A. Tassone, P. Imbriani, S. Cerri, G. Martella, P. Bonsi, A. Bellucci, A. Pisani, Alpha-synuclein is involved in DYT1 dystonia striatal synaptic dysfunction, Mov. Disord. 37 (2022) 949–961, https://doi.org/10.1002/mds.29024.
[44] D. Trudler, S. Sanz-Blasco, Y.S. Eisele, S. Ghatak, K. Bodhinathan, M.W. Akhtar, W. P. Lynch, J.C. Piña-Crespo, M. Talantova, J.W. Kelly, S.A. Lipton, α-synuclein oligomers induce glutamate release from astrocytes and excessive extrasynaptic NMDAR activity in neurons, thus contributing to synapse loss, J. Neurosci. 41 (2021) 2264–2273, https://doi.org/10.1523/JNEUROSCI.1871-20.2020.
[45] J.E. Lee, H.N. Kim, D.-Y. Kim, Y.J. Shin, J.Y. Shin, P.H. Lee, Memantine exerts neuroprotective effects by modulating α-synuclein transmission in a parkinsonian model, Exp. Neurol. 344 (2021), 113810, https://doi.org/10.1016/j.expneurol.2021.113810.

[46] M. Mellone, F. Gardoni, Glutamatergic mechanisms in l-DOPA-induced dyskinesia and therapeutic implications, J. Neural Transm. 125 (2018) 1225–1236, https://doi.org/10.1007/s00702-018-1846-8.
[47] P.J. Teravskis, A. Covelo, E.C. Miller, B. Singh, H.A. Martell-Martínez, M. A. Benneyworth, C. Gallardo, B.R. Oxnard, A. Araque, M.K. Lee, D. Liao, A53T mutant alpha-synuclein induces Tau-dependent postsynaptic impairment independently of neurodegenerative changes, J. Neurosci. 38 (2018) 9754–9767, https://doi.org/10.1523/JNEUROSCI.0344-18.2018.
[48] Y.C. Wong, K. Luk, K. Purtell, S. Burke Nanni, A.J. Stoessl, L. Trudeau, Z. Yue, D. Krainc, W. Oertel, J.A. Obeso, L.A. Volpicelli-Daley, Neuronal vulnerability in Parkinson disease: Should the focus be on axons and synaptic terminals? Mov. Disord. 34 (2019) 1406–1422, https://doi.org/10.1002/mds.27823.